Chapter

18 Neuroimaging in the evaluation of pattern and timing of fetal and neonatal brain abnormalities

Patrick D. Barnes

Introduction

In this updated review, current and advanced neuroimaging technologies are discussed, along with the basic principles of imaging diagnosis and guidelines for utilization in fetal, perinatal, and neonatal brain abnormalities [1,2]. This includes pattern of injury and timing issues, with special emphasis on neurovascular disease and the differential diagnosis. In the causative differentiation of static encephalopathies (e.g., cerebral palsy, CP) from progressive encephalopathies, specific categories and timing are addressed. These include developmental abnormalities, trauma, neurovascular disease, infections and inflammatory processes, and metabolic disorders. Although a rare but important cause of progressive perinatal encephalopathy, neoplastic processes are not considered in detail here. Molecular and genetic technologies continue to advance toward eventual clinical application.

Neuroimaging technologies and general utilization

Imaging modalities may be classified as structural or functional [1–12]. **Structural imaging** modalities provide spatial resolution based primarily on anatomic or morphologic data. **Functional imaging** modalities provide spatial resolution based upon physiologic, chemical, or metabolic data. Some modalities may actually be considered to provide both structural and functional information.

Ultrasonography (US) is primarily a structural imaging modality with some functional capabilities (e.g., Doppler: Fig. 18.1a,b) [1–8,13–26]. It is readily accessible, portable, fast, real-time and multiplanar. It is less expensive than other cross-sectional modalities and relatively non-invasive (non-ionizing radiation). It requires no contrast agent and infrequently needs patient sedation. The resolving power of US is based on variations in acoustic reflectance of tissues. Its diagnostic effectiveness, however, continues to be dependent upon the skill and experience of the operator and interpreter, and there are issues regarding inter-observer reliability and accuracy [1–8,13–26]. Also, US requires a window or path unimpeded by bone or air for cranial and spinal imaging. The most common uses of US are (1) fetal and neonatal screening, (2) screening of the infant who cannot be examined in the radiology department (e.g., premature neonate with intracranial hemorrhage, ECMO, intraoperative), (3) when important adjunctive information is quickly needed (e.g., cystic versus solid, vascularity, vascular flow [Doppler: Fig. 18.1a,b], or increased intracranial pressure), and (4) for real-time guidance and monitoring of invasive diagnostic or therapeutic surgical and interventional procedures [1–8,13].

In recent years, advanced US techniques have been introduced into clinical practice [1–8,13]. The development of high-resolution transducers, improvements in color Doppler signal processing, and new scanning techniques have significantly improved our ability to visualize structural, vascular, and cerebrospinal fluid abnormalities in the neonatal brain. Examples are the mastoid view to better visualize the posterior fossa, power Doppler and transcranial Doppler (TCD) to evaluate intracranial hemodynamics (e.g., resistive indices, RI: Fig. 18.1a,b), and the graded fontanel compression Doppler technique to evaluate hydrocephalus. Another advance in US technology that has yet to be translated is the development of vascular US contrast agents to amplify reflected sound waves. Potential applications include the detection of slow flow and the assessment of organ perfusion. Computerized analysis of textural features is another development that has promised increased sensitivity and specificity, but has not been translated to clinical practice [13].

Computed tomography (CT) is also primarily a structural imaging modality that has some functional capabilities (e.g., CT angiography) [1–8]. Although using ionizing radiation, current-generation multidetector CT (MDCT) effectively collimates and restricts the x-ray exposure to the immediate volume of interest, particularly when using the ALARA standard for pediatric patients, which adjusts radiation dose relative to age, size, and anatomic region [27]. Direct imaging is usually restricted to the axial plane (Fig. 18.1c–e). Reformatting from axial sections to other planes (e.g., coronal or sagittal) is now the MDCT standard. Projection scout images may provide information similar to plain films but with less spatial resolution. CT of the pediatric CNS is usually done using either the conventional or the helical/spiral technique. CT

Fetal and Neonatal Brain Injury, 4th edition, ed. David K. Stevenson, William E. Benitz, Philip Sunshine, Susan R. Hintz, and Maurice L. Druzin. Published by Cambridge University Press.

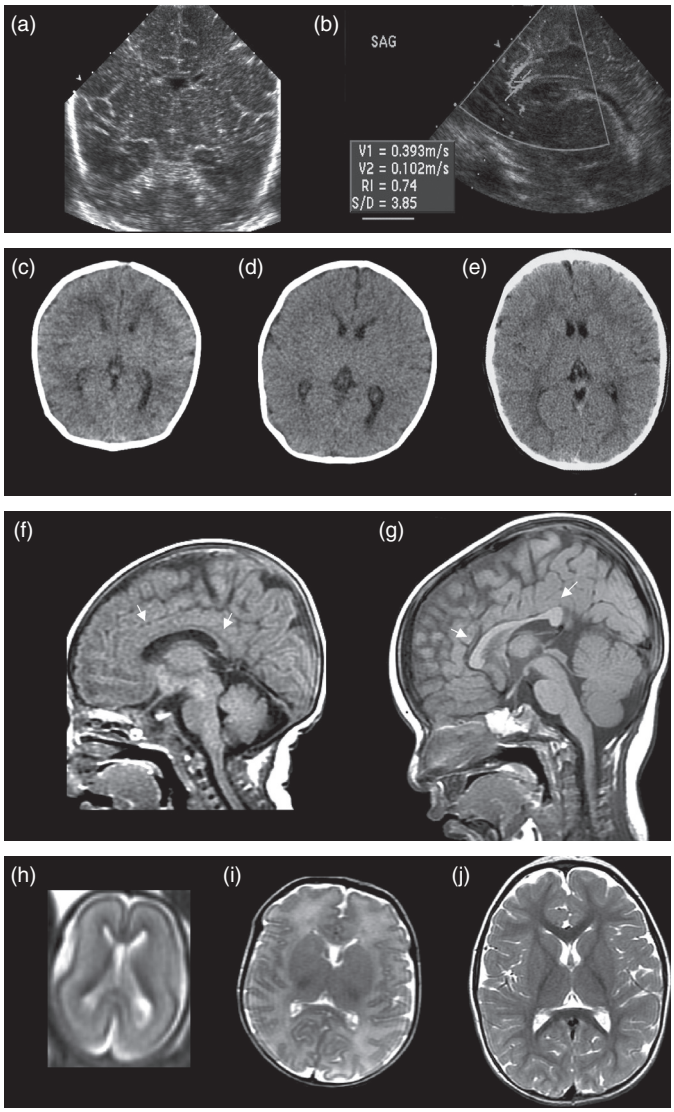

Fig. 18.1. Normal infant and child brain. Ultrasound (US) images of term neonate: (a) coronal US; (b) sagittal US + Doppler with resistive indices (RI). Computed tomography (CT) images of (c) term neonate, (d) 2-month-old infant, and (e) 2-year-old child show progress of maturation, including myelination. Sagittal T1 magnetic resonance images (MRIs) of (f) term neonate and (g) 1-year-old infant show progress in brain growth, myelination of the corpus callosum (arrows), and pituitary maturation. T2 MRIs of (h) 20-week fetus, (i) term neonate, and (j) 2-year-old child show progress in maturation, i.e., decreasing water content, increasing myelination and cortication. *See color plate section.*

requires sedation in infants and young children more often than does US but less often than MRI. The more rapid MDCT technology, however, has allowed a significant reduction in the need for sedation or anesthesia. The neonate or very young infant, for example, may be examined bundled while asleep after a feeding or during a nap. CT occasionally needs intravenous iodinated contrast enhancement, but cerebrospinal (CSF) contrast opacification is rarely needed. High-resolution bone and soft-tissue algorithms are important for demonstrating fine anatomy (e.g., skull base). Advances in computer display technology include image fusion, two-dimensional reformatting, three-dimensional volumetric and reconstruction methods, segmentation, and surface rendering techniques. These high-resolution display techniques are used for CT angiography and venography, craniofacial and spinal imaging for surgical planning, and stereotactic image guidance of radiotherapy, interventional, and neurosurgical procedures.

The role of CT has been further redefined in the context of accessible and reliable US and MRI [1–12,15,28,29]. US is the procedure of choice for primary imaging or screening of the brain and spinal neuraxis in the neonate and young infant. When US does not satisfy the clinical inquiry, or an acoustic window is not available, then CT becomes the primary modality for brain imaging in children, especially in acute or emergent presentations. This is especially important for acute neurologic presentations. In these situations, CT is primarily used to screen for acute or subacute hemorrhage, focal or diffuse edema, herniation, fractures, hydrocephalus, tumor mass, or abnormal collection (blood, pus, air, CSF, etc.). Other primary indications for CT include the evaluation of bony or air-space abnormalities of the skull base, cranial vault, orbit, paranasal sinuses, facial bones, and temporal bone. Additionally, CT is the definitive procedure for detection and confirmation of calcification. It is also important in the bony evaluation of a localized spinal column abnormality (e.g., trauma). Contraindications to CT in childhood are unusual, particularly with the proper application of radiation protection (ALARA standard), the appropriate use of non-ionic contrast agents, the proper administration of sedation or anesthesia, and the use of vital monitoring.

When CT is used, intravenous enhancement for blood pool effect (e.g., CT angiography) or blood–brain barrier disruption is additionally recommended for the evaluation of suspected or known vascular malformation, neoplasm, abscess, or empyema [1–4,28,29]. Enhanced CT may help evaluate a mass or hemorrhage of unknown etiology and identify the membrane of a chronic subdural collection. By identifying the cortical veins, enhanced CT may distinguish prominent low-density subarachnoid collections (benign extracerebral collections or benign external hydrocephalus of infancy) from low-density subdural collections (e.g., chronic subdural hematomas or hygromas). It also may help differentiate infarction from neoplasm or abscess, serve as an indicator of disease activity, for example in degenerative or inflammatory disease and vasculitis, or provide a high-yield guide for stereotactic or open biopsy. Ventricular or subarachnoid CSF-contrast opacification may further assist in evaluating or confirming CSF compartment lesions or communication (e.g., arachnoid cyst or ventricular encystment). As a rule, MRI is the preferred alternative to contrast-enhanced CT in the circumstances just enumerated.

Nuclear Medicine (NM) is primarily a functional imaging technology [1–8]. NM involves imaging of the biological distributions of administered radioactive pharmaceuticals. Whereas positron emission tomography (PET) has the unique ability to provide specific metabolic tracers (e.g., oxygen utilization and glucose metabolism) the wider availability, relative

simplicity, and rapid technical advancement of single photon emission computed tomography (SPECT) allows more practical functional assessment of the pediatric CNS. Clinical and investigative applications have included the assessment of brain development and maturation, focus localization in refractory childhood epilepsy (e.g., ictal perfusion SPECT, interictal PET), assessment of tumor progression versus treatment effects in childhood CNS neoplasia (perfusion and thallium SPECT, ^{18}FDG-PET), the evaluation of occlusive cerebrovascular disease for surgical revascularization (e.g., perfusion SPECT), the diagnosis of brain death (perfusion SPECT), the use of brain activation techniques (e.g., perfusion SPECT, PET) in the elucidation of childhood cognitive disorders, the assessment of CSF kinetics (e.g., in hydrocephalus, CSF leaks), and spinal-column screening (skeletal SPECT) [1–8].

Magnetic resonance imaging (MR, MRI) is both a structural and functional imaging modality [1–12]. MRI uses magnetic fields and radio waves. It is one of the less invasive or relatively non-invasive imaging technologies (Fig. 18.1f–j). Furthermore, the MRI signal is exponentially derived from multiple parameters (e.g., T1, T2, proton density, T2*, proton flow, proton relaxation enhancement, chemical shift, magnetization transfer, and molecular diffusion). MRI also employs many more basic imaging techniques than other modalities (e.g., spin echo, inversion recovery, gradient echo, and chemical shift imaging methods). Advancing MRI capabilities have further improved its sensitivity, specificity, and efficiency [1–12,30]. These include the fluid attenuation inversion recovery technique (FLAIR), fat-suppression short TI inversion recovery imaging (STIR), and magnetization transfer imaging (MTI) for increased structural resolution. Fast and ultrafast MRI techniques (fast spin echo, fast gradient echo, echo planar imaging, parallel imaging) have also been developed to reduce imaging times, improve structural resolution, and provide functional resolution (e.g., fetal imaging). Important applications include MR vascular imaging (MR angiography and venography, MRA) and perfusion MRI (PMRI), diffusion-weighted imaging (DWI), CSF flow and brain/cord motion imaging, brain activation techniques, and MR spectroscopy (MRS). Fast and ultrafast imaging techniques are also being used for fetal/obstetrical imaging [31–36], morphometrics, treatment planning, and "real-time" MRI-guided surgical and interventional procedures.

The role of MRI in imaging of the developing CNS is defined by its superior sensitivity and specificity in a number of areas as compared to US and CT [1–12,15,19–24,26,28–36]. MRI has also obviated or redefined the roles of invasive procedures (e.g., myelography, ventriculography, cisternography, angiography). MRI provides multiplanar imaging with equivalent resolution in all planes without repositioning the patient. Bone does not interfere with soft-tissue resolution, although metallic objects often produce signal void or field distortion artifacts. Some ferromagnetic or electronic devices (e.g., ferrous aneurysm clips and pacemakers) pose a hazard, and MRI is usually contraindicated in these cases. MRI usually requires longer exam times than does US and CT, and patient sedation or anesthesia is often required in infants and younger children, since image quality is easily compromised by motion. However, MRI may be successfully done in a large percentage of stable neonates and young infants using the "bundle and feed" technique. MRI may not be as readily accessible to the critically ill pediatric patient as is US or CT, and it may not be feasible in emergencies or for intensive care cases unless magnet-compatible vital monitoring and support is available. This is particularly important for the unstable neonate (e.g., using an MRI-compatible incubator) [12] (Fig. 18.2a).

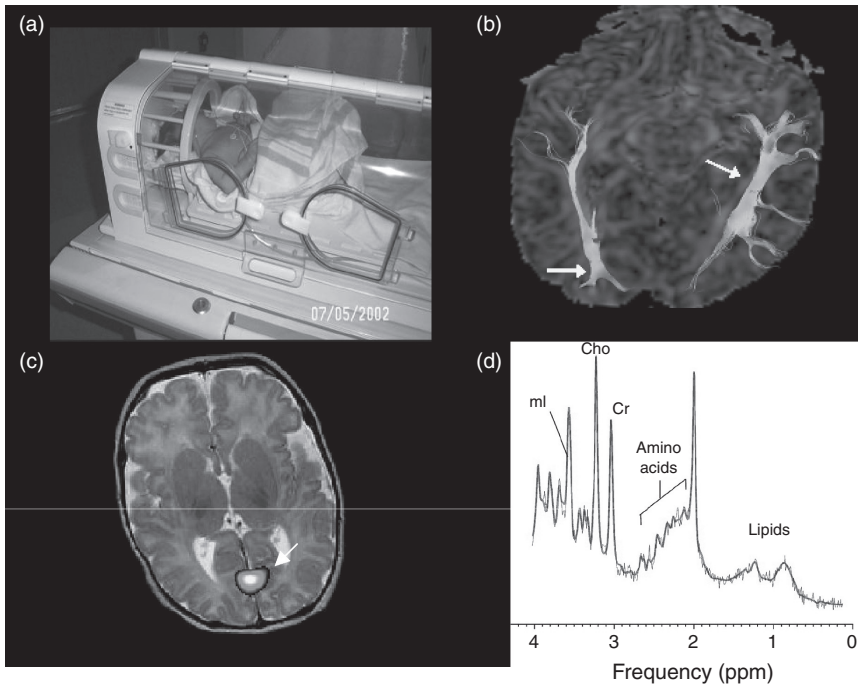

Fig. 18.2. Advanced MRI techniques: (a) MR-compatible incubator; (b) DTI white-matter tractography (arrows); (c) fMRI (primary visual cortex activation: arrow); (d) MR spectroscopy (see text). *See color plate section.* Courtesy of Ashok Panigrahy, MD, Children's Hospital Los Angeles [12].

MRI demonstrates superior sensitivity and specificity in a number of circumstances, particularly with the addition of new structural and functional techniques such as FLAIR, STIR, MTI, DWI, PMRI, and MRS [1–12,15,19–24,26,28–36]. The **FLAIR** sequence attenuates the signal from flowing water (i.e., CSF) and increases the conspicuity of non-fluid-water-containing lesions lying in close approximation to the CSF-filled subarachnoid and ventricular spaces. The **STIR** technique suppresses fat signal to provide improved conspicuity of water-containing lesions in regions where fat dominates (e.g., orbit, head and neck, spine). The **MTI** method suppresses background tissues and increases conspicuity for vascular flow enhancement (e.g., MRA) and gadolinium enhancement.

MRI is the imaging modality of choice in a number of clinical situations [1–12,15,19–24,26,28–36]. These include developmental delay (e.g., static encephalopathy vs. neurodegenerative disease); unexplained seizures (especially focal), unexplained neuroendocrine disorder, or unexplained hydrocephalus; the pretreatment evaluation of neoplastic processes and the follow-up of tumor response and treatment effects; suspected infectious, postinfectious, and other inflammatory or non-inflammatory encephalitides (e.g., encephalitis, postinfectious demyelination, vasculitis); migrational and other submacroscopic dysgeneses (e.g., cortical dysplasia); neurocutaneous syndromes (e.g., neurofibromatosis 1, tuberous sclerosis); intractable or refractory epilepsy; vascular diseases, hemorrhage, and the sequelae of trauma.

MRI frequently offers greater diagnostic specificity than does CT or US for delineating vascular and hemorrhagic processes. This includes the clear depiction of vascular structures and abnormalities based on proton flow parameters and software enhancements not requiring the injection of contrast agents (e.g., MRA). **MR angiography (MRA)** techniques may additionally be used to differentiate arterial from venous occlusive disease [1–12,15,19–24,26,28–36]. Using gradient recalled echo (GRE) magnetic susceptibility techniques, MRI also provides more specific identification and staging of hemorrhage and clot formation according to the evolution of hemoglobin breakdown. MRI is often reserved for more definitive evaluation of hemorrhage and as an indicator or guide for angiography in a number of special situations. MRI may be used to evaluate an atypical or unexplained intracranial hemorrhage by distinguishing hemorrhagic infarction from hematoma and by distinguishing among the types of vascular malformations (e.g., cavernous vs. arteriovenous malformations). MRA may obviate the need in some cases of vascular malformation for conventional angiography in the follow-up of surgery, interventional treatment, or radiosurgery.

In the evaluation of intracranial vascular anomalies (e.g., vascular malformation, aneurysm), MRI may identify otherwise unsuspected prior hemorrhage (i.e., hemosiderin) [1–12,15,19–24,26,28–36]. When CT demonstrates a nonspecific focal high density (calcification vs. hemorrhage), MRI may provide further specificity, for example, by distinguishing an occult vascular malformation (e.g., cavernous malformation) from a neoplasm (e.g., glioma). It may further assist US or CT in differentiating benign infantile collections (i.e., external hydrocephalus) from subdural hematomas [28,29]. MRI often also provides definitive evaluation of muscular and cutaneous vascular anomalies (i.e., hemangiomas, vascular malformations) that arise in parameningeal locations (e.g., head and neck, paraspinal) and extend to involve the CNS directly or are associated with other CNS vascular or non-vascular abnormalities.

MR spectroscopy (MRS) offers a non-invasive in vivo approach to biochemical analysis [1–12,37–40] (Fig. 18.2d). Furthermore, MRS provides additional quantitative information regarding cellular metabolites, since signal intensity is linearly related to steady-state metabolite concentration. MRS can detect cellular biochemical changes prior to the detection of morphological changes by MRI or other imaging modalities. MRS may therefore provide further insight into both follow-up assessment and prognosis. With recent advances in instrumentation and methodology, and utilizing the high inherent sensitivity of hydrogen 1, single-voxel and multivoxel proton MRS is now carried out with relatively short acquisitions to detect low-concentration metabolites in healthy and diseased tissues. Phosphorus-31 spectroscopy has also been developed for pediatric use. Currently, MRS has been primarily used in the assessment of brain development and maturation (Fig. 18.3), perinatal brain injury, childhood CNS neoplasia versus treatment effects, and metabolic and neurodegenerative disorders [39–40].

Perfusion MRI (PMRI) has been developed to evaluate cerebral perfusion dynamics through the application of a dynamic contrast-enhanced T2*-weighted MR imaging technique [1–4,8,12,31,41]. This technique has been used to qualitate and quantitate normal and abnormal cerebrovascular dynamics of the developing brain by analyzing hemodynamic parameters including relative cerebral blood volume, relative cerebral blood flow, and mean transit time, all as complementary to conventional MR imaging. Non-contrast-enhanced methods of PMRI have also been developed (e.g., flow-activated inversion recovery, FAIR; arterial spin labeling, ASL; blood oxygen level determination, BOLD) [41]. Current and advanced applications of these perfusion techniques include the evaluation of ischemic cerebrovascular disease (e.g., hypoxia–ischemia, moyamoya, sickle cell disease), the differentiation of tumor progression from treatment effects, and brain activation imaging [1–4,8,12,31,41]. One of the most active areas of research is the localization of brain activity, an area previously dominated by NM including SPECT and PET.

Functional MRI (fMRI) is the terminology often applied to brain activation imaging in which local or regional changes in cerebral blood flow are displayed that accompany stimulation or activation of sensory (e.g., visual, auditory, somatosensory), motor, or cognitive centers [1–4,12]. fMRI is providing important information regarding the spatial distribution of sensory, motor, and cognitive function and functional impairment (Fig. 18.2c). Also, it may serve as a guide for safer and

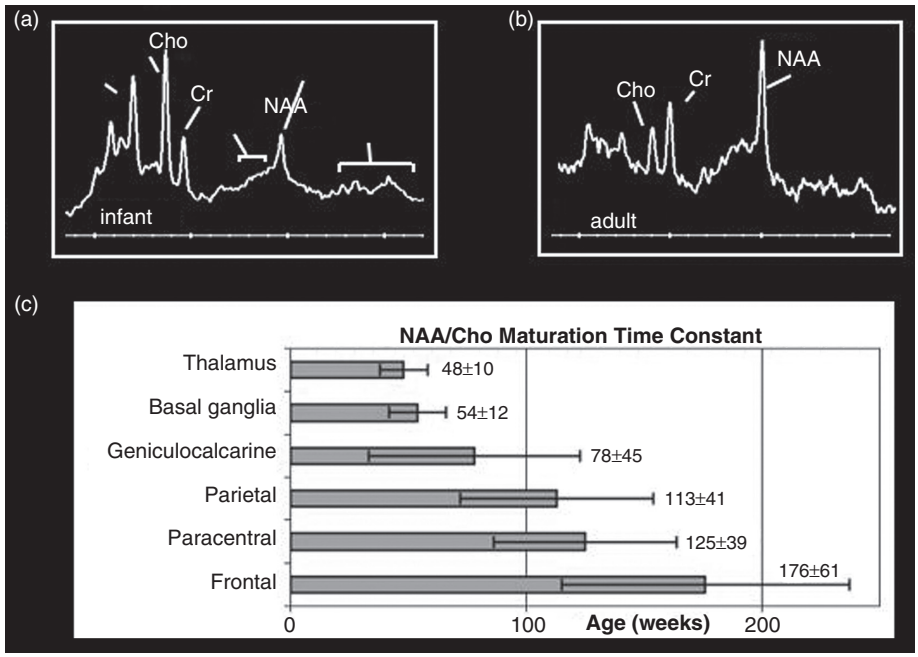

Fig. 18.3. H-1 MR spectroscopy of the developing brain with (a) infant spectra, (b) adult spectra, and (c) maturation time constants for brain regions. Dermon J, Barnes PD, Spielman D. Spatiotemporal mapping of cerebral maturation in childhood using 2D MR spectroscopic imaging. American Society of Neuroradiology, 2002.

more effective interventions including microneurosurgery or conformal radiotherapy, for example in the ablation of tumors, vascular malformations, and seizure foci. More recently, fMRI is being used to evaluate brain development and maturation in the neonate and young infant, including the effects of injury and post-injury repair and recovery [12].

Using echo planar or line-scan spin echo techniques, **diffusion-weighted imaging (DWI)** provides information based upon differences in the rate of diffusion of water molecules, and it is especially sensitive to cellular changes [1–12,30,40,42–53]. The rate of diffusion, or apparent diffusion coefficient (ADC), is higher for free or pure water than for macromolecular bound water. The ADC varies according to the microstructural or physiologic state of a tissue. Fractional anisotropy (FA) is a vector measurement of the directionality of diffusion using **diffusion tensor imaging** (**DTI**) methods and also varies with the microstructural environment, both developmentally and pathologically [53] (Fig. 18.2b). This method is especially helpful in assessing axonal development and injury, including myelination and synaptogenesis (connectivity). Current clinical applications of DWI and DTI include the assessment of brain maturation, the evaluation of acute injury, and the analysis of the sequelae of injury (Fig. 18.4). A particularly important application of DWI is in the early detection of diffuse and focal ischemic injury. The ADC of water is reduced within minutes of an ischemic insult and progressively so within the first hour. High-intensity abnormalities are demonstrated on DWI, along with low-intensity abnormalities on calculated ADC images, at a time when conventional MRI is negative, and this likely reflects cellular injury (e.g., necrosis) with primary or secondary energy failure. Further investigations are under way regarding the roles of DWI, PMRI, and MRS in the early diagnosis and treatment of potentially reversible ischemic injury.

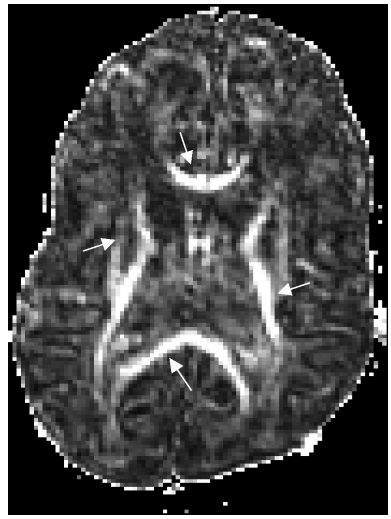

Fig. 18.4. DTI with FA map in preterm neonate as a quantitative display of white-matter development (arrows) of the internal capsule and corpus callosum [12].

Motion-sensitive MRI techniques are not only used to evaluate vascular flow (e.g., MRA) and perfusion, but may also be used to demonstrate the effect of pulsatile cardiovascular flow on other fluid tissues (e.g., CSF) and on non-fluid tissues such as the brain and spinal cord. Using cardiac or pulse gating, these MRI techniques may be used to evaluate, preoperatively and postoperatively, abnormalities of CSF dynamics (e.g., hydrocephalus, hydrosyringomyelia), as well as abnormalities of brain motion (e.g., Chiari malformation), and spinal cord motion (e.g., tethered cord syndrome) [1–4]. A number of non-gated MRI techniques (e.g., propeller imaging) are also being used to reduce motion artifact and improve image quality.

Guidelines and principles of imaging diagnosis

Developmental abnormalities

Congenital abnormalities of the CNS may be developmental or acquired in origin, and may result from defective formation, postformational destruction, or disordered maturation [1,2,4,5,54]. These are probably best classified according to gestational timing (Table 18.1), and include disorders of dorsal and ventral neural tube formation; disorders of neuronal, glial, and mesenchymal formation; neuroclastic processes (encephaloclastic, myeloclastic); and disorders of maturation (myelination and cortical maturation). These are classified in six groups (I–VI) in Table 18.1. Developmental anomalies often detected by US (prenatal or postnatal) or CT are the *gross* formational macrostructural defects of categories I–IV and the *gross* neuroclastic macrostructural lesions of category V [1,2,4,5,54]. However, MRI always provides more complete delineation of these defects. This is especially true for those abnormalities involving the ventricular system or containing CSF. These include cephaloceles (Fig. 18.5), hydrocephalus, hydranencephaly, holoprosencephaly, absent septum pellucidum, hypogenesis of the corpus callosum (Figs. 18.5–18.7), porencephaly, open schizencephaly, the Dandy–Walker–Blake spectrum (Fig. 18.7), and arachnoid cysts. US may not clearly distinguish hydranencephaly (absent cerebral mantle) from severe hydrocephalus (attenuated cerebral mantle). This is usually clarified by CT or MRI (Fig. 18.8). Other gross macrostructural anomalies often detected by US or CT include Chiari II malformation, lissencephaly, and vascular malformations such as the Galenic malformation. Any "cystic" lesion detected by US should be examined with Doppler to determine if it is vascular in nature. Neuroclastic processes are destructive lesions of the already formed CNS and may result from a variety of prenatal or perinatal insults including hypoxia–ischemia and infection (Table 18.1). MRI may often demonstrate subtle macrostructural abnormalities not revealed by US or CT (e.g., periventricular leukomalacia) [1–12,15,17,19–24,26,33].

MRI is important when the US or CT fails to satisfy the clinical investigation. MRI often provides a more complete delineation of complex macrostructural CNS anomalies for diagnosis, treatment, prognosis, and genetic counseling [1,2,4,5,33,54]. In fact, ultrafast MRI techniques are being increasingly used prenatally to evaluate for fetal CNS abnormalities in at-risk pregnancies or as detected by obstetrical US [31–36] (Figs. 18.5–18.7). Furthermore, MRI is often indicated if more specific treatment is planned beyond simple shunting of hydrocephalus. Intraoperative guidance may be provided by real-time and Doppler US. Patients with craniosynostosis are best evaluated with 3DCT. Those with multiple suture involvement, especially when it is associated with craniofacial syndromes, may require more extensive evaluation beyond 3DCT, including CT venography, MRI, and MR venography (jugular venous steno-occlusive disease with collateralization).

MRI is often required to structurally delineate the more subtle macrostructural anomalies arising as disorders of

Table 18.1. Classification of CNS malformations by gestational timing

I. Disorders of dorsal neural tube development (3–4 weeks)
Anencephaly
Cephaloceles
Dermal sinus
Chiari malformations
Spinal dysraphism
Hydrosyringomyelia
II. Disorders of ventral neural tube development (5–10 weeks)
Holoprosencephalies
Agenesis septum pellucidum
Optic and olfactory hypoplasia/aplasia
Pituitary – hypothalamic hypoplasia/aplasia
Cerebellar hypoplasia/aplasia
Dandy Walker spectrum
Craniosynostosis
III. Disorders of migration and cortical organization (2–5 months)
Schizencephaly
Neuronal heterotopia
Agyria/pachygyria
Lissencephaly
Polymicrogyria
Agenesis corpus callosum
IV. Disorders of neuronal, glial, and mesenchymal proliferation, differentiation, and histiogenesis (2–6 months)
Micrencephaly
Megalencephaly
Hemimegalencephaly
Aqueductal anomalies
Colpocephaly
Cortical dysplasias
Neurocutaneous syndromes
Vascular anomalies
Malformative tumors
Arachnoid cysts
V. Encephaloclastic processes (> 5–6 months)
Hydranencephaly
Porencephaly
Multicystic encephalopathy
Encephalomalacia
Leukomalacia
Hemiatrophy
Hydrocephalus
Hemorrhage
Infarction
VI. Disorders of maturation (7 months – 2 years)
Hypomyelination
Delayed myelination
Dysmyelination
Demyelination
Cortical dysmaturity

Note:
See references [2,4,54].

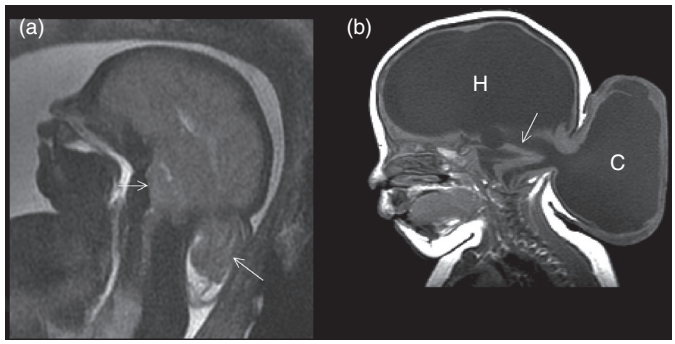

Fig. 18.5. (a) Fetal sagittal T2 MRI, showing cervico-occipital cephalocele (posterior arrow), Chiari III malformation (anterior arrow), agenesis of the corpus callosum, and microcephaly. (b) Neonatal sagittal T1 MRI, showing occipital meningoencephalocele (C) with kinked brainstem (arrow) and hydrocephalus (H).

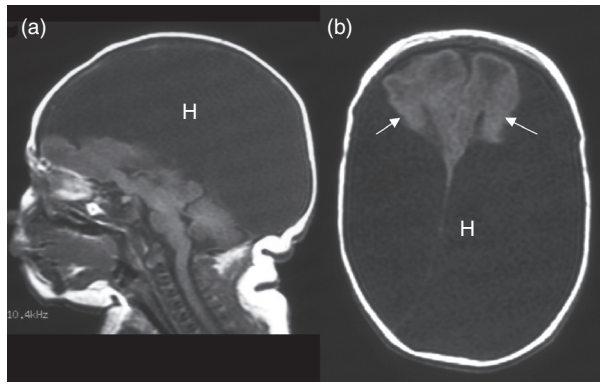

Fig. 18.8. Hydranencephaly on (a) sagittal and (b) axial T1 MRI. Only a small portion of cortex is present frontally (arrows).

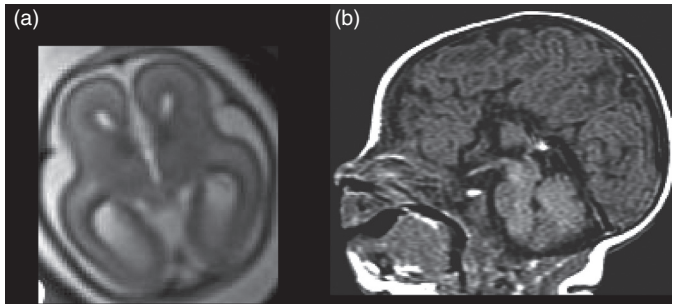

Fig. 18.6. Agenesis corpus callosum on (a) fetal axial T2 and (b) neonatal sagittal T1 MRI (see Fig. 18.1. f,g) [50].

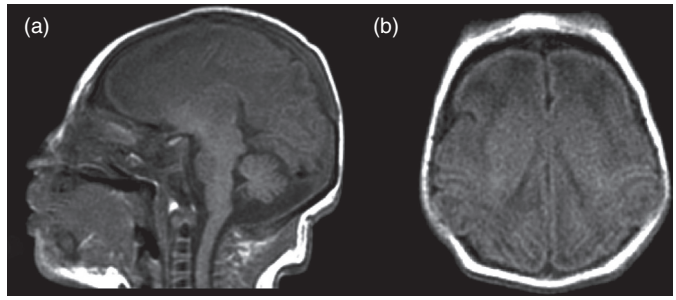

Fig. 18.9. Microlissencephaly: neonatal (a) sagittal and (b) axial T1 MRI, showing microcephaly with agyric cortex.

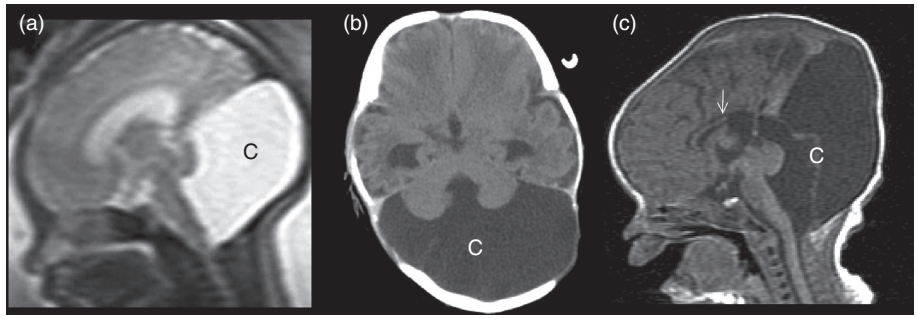

Fig. 18.7. Dandy–Walker cyst (C): (a) fetal sagittal T2 MRI; (b) neonatal axial CT; (c) sagittal T1 MRI with hypogenesis of the corpus callosum (arrow).

migration and cortical organization (category III: Fig. 18.9) or as disorders of proliferation, differentiation, and histiogenesis (category IV: Fig. 18.10) [1,2,4,5,33,54]. The perfusional and metabolic characteristics of these anomalies (e.g., focal cortical dysgenesis, hemimegalencephaly) may be investigated with SPECT and PET, respectively, in children with medically refractory partial epilepsy who are candidates for surgical ablation. For added precision, the SPECT or PET data may be fused with the MRI data to provide a higher-resolution spatial display of the functional information. MRS, DWI, DTI, and PMRI with fMRI are also contributing to the evaluation and treatment of these patients [4,12,30]. MRI is now the preferred modality for the screening and definitive evaluation of the dysgenetic, neoplastic, and vascular manifestations of the neurocutaneous syndromes (Fig. 18.11). After initial screening with US or CT, MRI is also considered the primary technology for treatment planning and follow-up of vascular malformations and developmental tumors [1,2,4,30]. Although arachnoid cysts are often readily delineated by US or CT, MRI is usually necessary for confirmation (i.e., to exclude solid tumor) and for surgical planning. FLAIR or DWI may readily distinguish an arachnoid cyst from other lesions (e.g., dermoid–epidermoid, fibrillary astrocytoma). Maturation (i.e., myelination and cortical maturation) and disorders of maturation (category VI) may be precisely assessed only by MRI [1,2,4,5,30,33,54] (Fig. 18.1f–j). The MRI findings,

Fig. 18.10. Hemimegalencephaly: neonatal axial T2 MRI shows larger right hemisphere with unilateral ventriculomegaly and abnormal cortication.

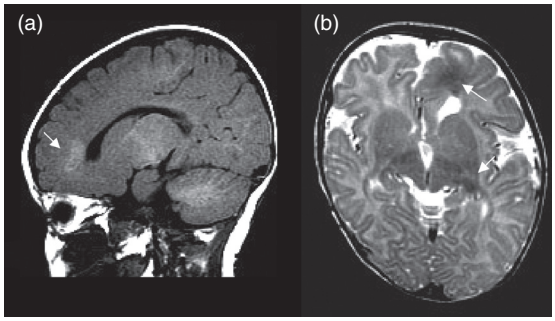

Fig. 18.11. Tuberous sclerosis with periventricular and subcortical tubers (arrows) on (a) neonatal sagittal T1 and (b) axial T2 MRI.

however, are often non-specific regarding causation, particularly in the first year of life, because of the watery character of the immature brain. DTI and MRS may add specificity to the diagnostic evaluation of these infants [1–12,37–40] (Figs. 18.2–18.4).

Neurovascular disease

Neurovascular disease characteristically presents as an acute neurologic event (e.g., neonatal encephalopathy). However, a recently discovered but fixed deficit (e.g., hemiplegia, spastic diplegia, hypotonia) may be the first indication of a remote prenatal or perinatal neurovascular injury. Imaging assists in the clinical evaluation and differentiation of hypoxia–ischemia, hemorrhage, and occlusive vascular disease [1–12,30].

Hypoxia–ischemia

In general, the pattern of injury associated with hypoxic–ischemic encephalopathy (HIE), or other insults (e.g., reperfusion), varies with the severity and duration of the insult as well as with the gestational (or corrected) age (GA) of the fetus, neonate, or infant at the time of the insult or insults [1–12] (Table 18.2). Different brain structures are more vulnerable than others to the different types of HIE insults (e.g., partial prolonged, profound, combined) at different stages of brain development (e.g., formational vs. postformational GA, preterm vs. term vs. full-term or post-term GA). Brain tissues in the arterial border zones or watersheds (intervascular boundary zones), brain tissues with high metabolic demands, mature or actively maturing tissues, and tissues with higher concentrations of neuroexcitatory amino acids are particularly vulnerable to HIE and to other insults (e.g., hypoglycemia, trauma, infection, seizures) [1–12,55–61]. Prenatal or perinatal partial prolonged HIE (e.g., one or more insults of hypoxia/hypoperfusion) may be associated with periventricular border-zone/watershed injury to the preterm fetus or neonate (e.g., 27–35 weeks GA) [1–12,55,57,62–75]. Subtypes of white-matter injury of prematurity (i.e., "encephalopathy of prematurity") include the classic focal/multifocal "cystic" type of periventricular leukomalacia (PVL), the focal/multifocal "noncystic" (gliotic) form of PVL, and the diffuse white-matter gliosis injury pattern (Figs. 18.12–18.15). The pathogenesis may include not only hypoxia–ischemia but other factors such as infectious or inflammatory processes (e.g., maternal infection, chorioamnionitis, funisitis, fetal inflammatory response, cytokine-mediated injury) whether occurring in the preterm, or term, fetus or neonate [7,66,70]. Prenatal or perinatal partial prolonged HIE during term gestation (e.g., 37–42 weeks GA) may produce a cortical and subcortical border-zone/watershed cerebral injury (Figs. 18.16, 18.17). A transitional partial prolonged HIE pattern (cortical/subcortical/periventricular) may be seen in the late preterm to early mid-term GA (e.g., 36–38 weeks) or with more severe injuries. Fetal or neonatal brain injury may also occur with more profound HIE insults (e.g., anoxia or circulatory arrest) and involve the thalami, basal ganglia (especially putamina), brainstem (especially midbrain), cerebellar vermis,

Table 18.2. Imaging patterns of hypoxic–ischemic encephalopathy (HIE)

Hemorrhage
Germinal matrix – intraventricular hemorrhage
Choroid plexus – intraventricular hemorrhage
Subarachnoid hemorrhage
Hemorrhagic infarctions
Partial prolonged HIE
Preterm: White-matter injury of prematurity (e.g., periventricular leukomalacia)
Term/full-term/post-term: Cortical/subcortical injury (borderzone, watershed, parasagittal)
Intermediate: combined or transitional pattern
Ulegyria
Cystic encephalomalacia
Profound HIE
Thalamic and basal ganglia injury
Brainstem injury
Cerebellar vermian injury
Hippocampal injury
Cerebral white-matter injury
Paracentral injury
Global injury (prolonged profound)
Combined profound and partial prolonged (or prolonged profound) HIE
Total asphyxia pattern (including cystic encephalomalacia)

Notes:
Depends on gestational age, chronological age, duration and severity of the insult.
See references [2–8].

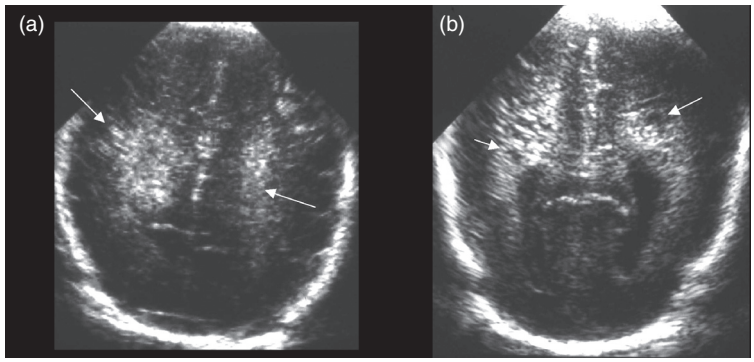

Fig. 18.12. Cystic PVL: (a) US, acute edema phase (confluent increased echoes – arrows); (b) US, subacute cystic phase (hypoechoic foci with surrounding increased echoes – arrows).

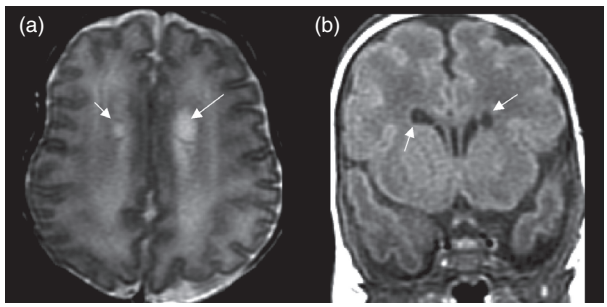

Fig. 18.13. Cystic PVL: (a) axial T2 and (b) coronal FLAIR MRI, chronic cystic phase (arrows).

hippocampi, paraventricular white matter, and perirolandic cortex [1–12,55,57,76–80] (Figs. 18.18, 18.19). This type of injury may also vary with GA (thalamic greater than putaminal involvement in the preterm GA; putaminal, hippocampal, and paracentral injury more common in the term GA). Combined partial prolonged plus profound HIE patterns (e.g., total asphyxia) may also occur [1–12,76–80] (Fig. 18.20).

US, CT, or MRI (e.g., DWI) may demonstrate evolving edema, necrosis, or hemorrhage in the hyperacute, acute, and subacute phases [1–12] (Figs. 18.12–18.20). The edema of non-hemorrhagic HIE (e.g., partial prolonged type) usually evolves over 1–7 days and often peaks between 36 and 72 hours (2–4 days by US, CT) following the insult(s) and depending upon reperfusion (and other "insults"). US may show hyperechogenicity, and CT may show hypodensities with decreased gray–white matter differentiation. Complete loss of gray–white differentiation may correlate with peak edema [60,61]. In the early phases of the injury, the neuroimaging findings may be non-specific as to causation. The differential diagnosis includes HIE, multifocal occlusive vascular infarction, infection, metabolic derangement (e.g., hypoglycemia, hyperbilirubinemia, fluid-electrolyte imbalance), metabolic or connective tissue disorder, and venous thrombosis (e.g., coagulopathy) [1–12]. Associated hemorrhage may be subarachnoid, germinal matrix and intraventricular hemorrhage (e.g., preterm fetus or neonate), choroid plexus/intraventricular hemorrhage (e.g., term fetus or neonate), and cerebral or cerebellar hemorrhage (e.g., hemorrhagic infarction). Their imaging characteristics are described in the next section.

According to the evidence-based medical literature, the sensitivity and specificity of MRI depends on the techniques used and the timing of the imaging [2,4,6,40,45,78]. Conventional MRI may show characteristic T1 hypointensities/T2 hyperintensities (12–48 hours), followed by T1 hyperintensities (as early as 2–4 days), and then T2 hypointensities (as early as 6–7 days). These T1 and T2 changes may last for a number of weeks to a month. DWI may be abnormal before conventional MRI and show restricted diffusion with decreased ADC as increased intensity on DWI and decreased intensity on ADC maps [2,8,40,45]. Diffusion abnormalities may tend to evolve for up to 2–3 weeks. Knowledge of these evolving intensity features is particularly important in order to avoid misinterpretation regarding pattern of injury and timing [40]. Doppler with resistive indices (e.g., RI < 60) or MRS (e.g., elevated lactate, elevated glutamate, elevated lipids, decreased *N*-acetyl-aspartate [NAA]) may provide additional early indicators of timing and outcome [2,6,8,14,37,40,81]. The more subtle ischemic PVL lesions (e.g., cystic phase) may be better delineated by US (2–6 weeks after insult(s)) than by CT or MRI, in which the density and intensity character of immature

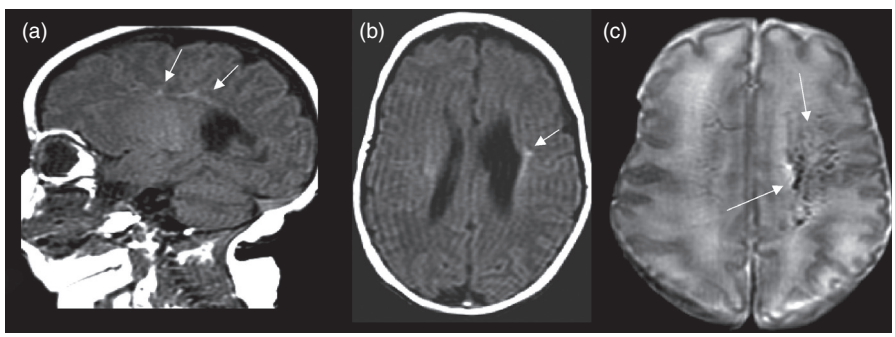

Fig. 18.14. Non-cystic PVL with foci of gliosis (arrows) as high intensities on (a) sagittal and (b) axial T1 MRI, plus mineralization or hemorrhages (arrows) as low intensities on (c) axial GRE MRI.

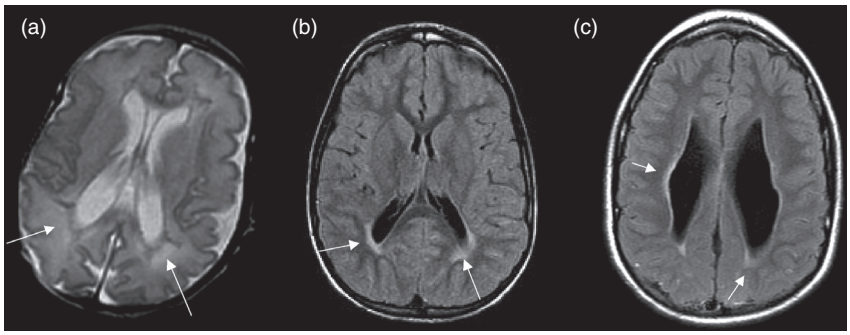

Fig. 18.15. Diffuse PVL (high intensities – arrows) on (a) near-term axial T2 and (b,c) older infant axial FLAIR MRI.

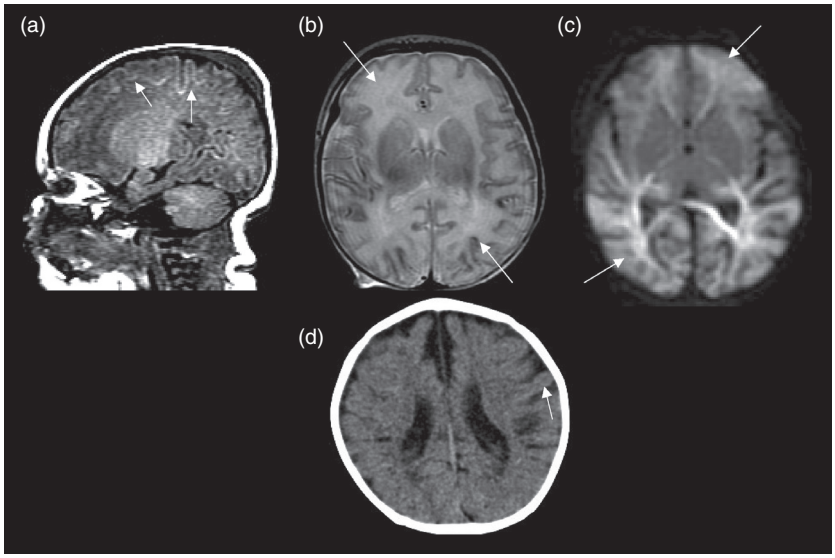

Fig. 18.16. Partial prolonged HIE: acute phase with watershed injury (arrows) on (a) sagittal T1, (b) axial T2, and (c) axial DWI; (d) chronic phase with cortical atrophy and ulegyria (arrow) on axial CT.

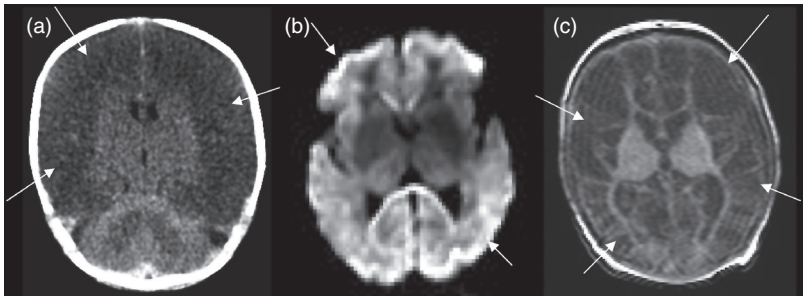

Fig. 18.17. Very severe partial prolonged HIE: acute–subacute phase with (a) low-density cerebral peak edema (arrows) on axial CT and (b) high-intensity cerebral restricted diffusion (arrows) on axial DWI; (c) chronic phase with cystic encephalomalacia (arrows) on axial T1.

white matter often obscures the injury. However, CT and MRI often show gray-matter injury better than US, and MRI demonstrates non-cystic white-matter injury better than US or CT [4,8,19–24,26]. Further developments of PMRI, DWI, and MRS have further improved the diagnostic sensitivity and specificity of MRI [4,8,12,30,40]. In fact, DWI has demonstrated restricted diffusion in the acute phase of PVL when US, CT, and conventional MRI are negative or non-specific. Such advances may facilitate the early institution of neuroprotective measures to treat potentially reversible primary injury (necrosis, apoptosis) and secondary injury (reperfusion, transneural degeneration) in HIE [82]. These advanced MRI techniques may also assist in distinguishing HIE from other causes of encephalopathy, including common metabolic derangements (e.g., hypoglycemia, hyperbilirubinemia), rarer inborn errors of metabolism, and non-metabolic conditions (e.g., infection).

The long-term result of HIE is a static encephalopathy (i.e., CP) and imaging may demonstrate injury in the chronic phases (> 14–21 days after the insult(s)) including porencephaly, hydranencephaly, atrophy, chronic periventricular leukomalacia, cystic encephalomalacia, gliosis, or mineralization in a characteristic distribution as described above [1–12] (Figs. 18.12–18.20). The chronic changes are best demonstrated by MRI. In general, for pattern of injury and timing purposes, two pieces of imaging evidence are optimally desired: (1) late imaging, and preferably MRI, beyond 2–3 years of age

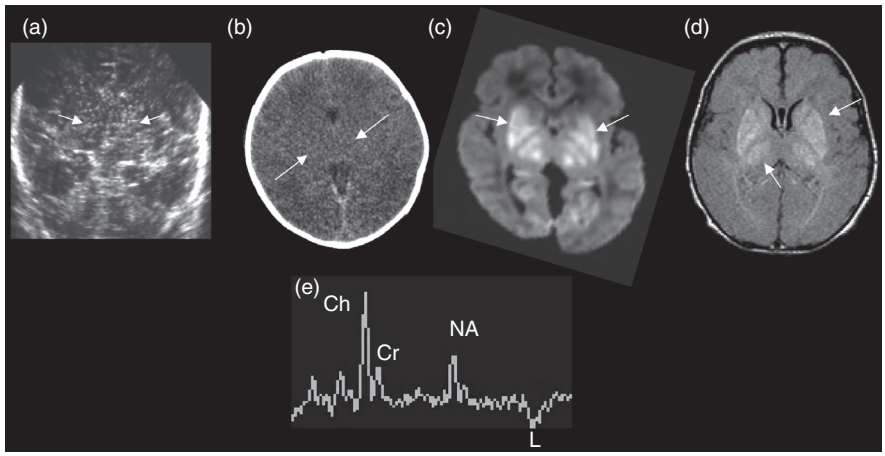

Fig. 18.18. Profound HIE: acute phase with (a) bilateral basal ganglia and thalamic hyperechogenicity (arrows) on US; (b) hypodensities (arrows) on CT; high intensities (arrows) on (c) axial DWI and (d) T1/FLAIR MRI; and (e) inverted lactate doublet (L) on MRS.

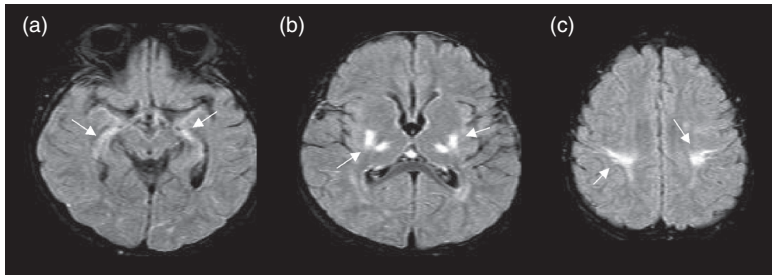

Fig. 18.19. Profound HIE: chronic phase with (a–c) bilateral hippocampal, putaminal, thalamic, and paracentral high intensities (arrows) on axial FLAIR MRI.

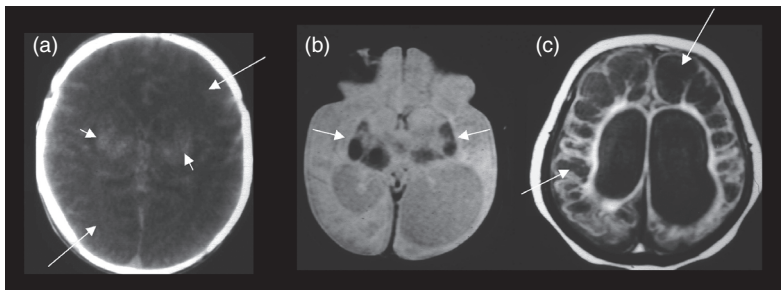

Fig. 18.20. Term combined HIE: subacute phase with (a) basal ganglia and thalamic high densities (short arrows) plus cerebral low densities (long arrows) on CT; chronic phase with (b) basal ganglia and thalamic hypointense mineralization (arrows) on axial GRE plus (c) hypointense cystic encephalomalacia (arrows) on axial T1 MRI.

when the brain is greater than 90% mature (no more water of immaturity), in order to get a final, permanent injury pattern for causative etiology and GA timing; and (2) early postnatal (and/or prenatal) imaging, and preferably MRI, in order to evaluate evolution in the acute, subacute, and chronic phases, so that timing as to "day range" relative to the perinatal and peripartum periods may be assessed [1–12,40].

Intracranial hemorrhage

Intracranial hemorrhage may result from parturitional trauma, HIE, a coagulopathy (e.g., thrombocytopenia, disseminated intravascular coagulopathy [DIC], extracorporal membrane oxygenation [ECMO]), vasoocclusive disease (e.g., thrombophilia with venous thrombosis), or it may be idiopathic [1–12,28,29,83]. Hemorrhage may occasionally be associated with infection (e.g., herpes simplex virus 2). Vascular malformations producing intracranial hemorrhage are rare in the neonate and young infant and usually not encountered until later childhood (i.e., arteriovenous malformations [AVM], cavernous malformations, developmental venous anomalies, and telangiectasias) [1–12,28,29]. Aneurysms are exceedingly rare in children but may be developmental, associated with a syndrome (e.g., Turner syndrome), or related to trauma (e.g., dissection) or infection (i.e., mycotic aneurysm). The vein of Galen malformations are subclassified as choroidal, mural, and AVM types. They rarely hemorrhage, and more commonly present in infancy with congestive heart failure, cerebral ischemia, or hydrocephalus.

US or CT remains the primary imaging choice in acute situations [1–12,29]. As mentioned above, there may be subarachnoid hemorrhage, germinal matrix and intraventricular hemorrhage (e.g., premature fetus or neonate), choroid plexus/intraventricular hemorrhage (e.g., term fetus or neonate), and cerebral or cerebellar hemorrhage (e.g., hemorrhagic infarction). The hemorrhage usually appears hyperechoic on US and high-density on CT in the acute to subacute phases (range 3 hours – 7 days) unless there is associated coagulopathy. With evolution and resolution, the hemorrhage

Table 18.3. MRI of intracranial hemorrhage and thrombosis

Stage	Biochemical form	Site	T1 MRI	T2 MRI
Hyperacute (+ edema) [< 12 hours]	Fe II oxy Hb	Intact RBCs	Isointense–Low i	High i
Acute (+ edema) [1–3 days]	Fe II deoxy Hb	Intact RBCs	Isointense–Low i	Low i
Early subacute (+ edema) [3–7 days]	Fe III met Hb	Intact RBCs	High i	Low i
Late subacute (− edema) [1–2 weeks]	Fe III met Hb	Lysed RBCs (extracellular)	High i	High i
Early chronic (− edema) [> 2 weeks]	Fe III transferrin	Extracellular	High i	High i
Chronic (cavity)	Fe III ferritin and hemosiderin	Phagocytosis	Isointense–Low i	Low i

Notes:
RBCs, red blood cells; +, present; −, absent; Hb, hemoglobin; Fe II, ferrous; Fe III, ferric.
See references [2,4,29,84,98].

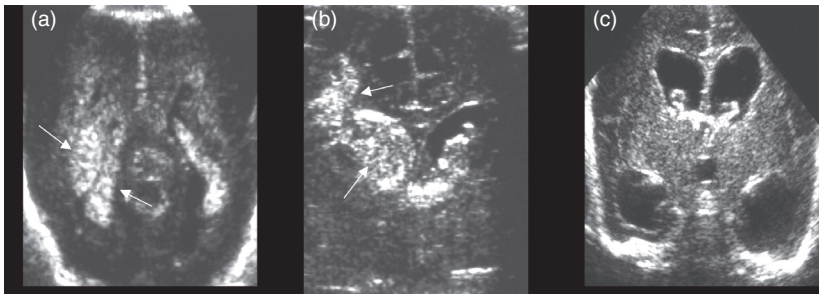

Fig. 18.21. (a) Hyperechoic grade III and (b) grade IV GMH–IVH (arrows), and (c) posthemorrhagic hydrocephalus on coronal US.

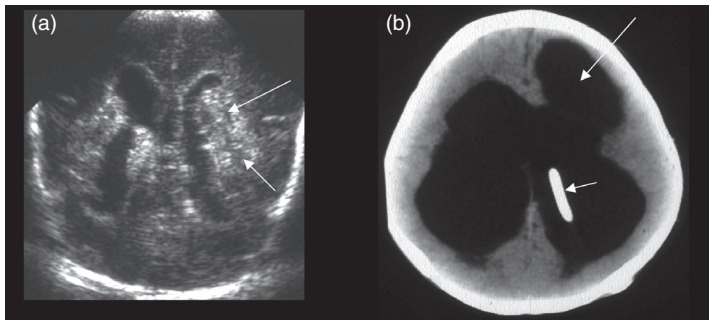

Fig. 18.22. (a) Hyperechoic grade IV IVH with periventricular hemorrhagic infarction (arrows) on coronal US; (b) posthemorrhagic hydrocephalus with porencephaly (long arrow) on axial CT with shunt catheter (short arrow).

becomes isoechoic to hypoechoic and isodense to hypodense (> 7–10 days).

MRI may offer more specific characterization of the hemorrhagic component with regard to timing (Table 18.3). Acute intracranial hemorrhage, particularly subarachnoid, may be specifically diagnosed by CT or lumbar puncture for CSF analysis. Although FLAIR may identify subarachnoid hemorrhage as hyperintensity and GRE may identify acute hemorrhage in any location as hypointensity, MRI often provides better specificity beyond the acute phases [2,4,29,84] (Table 18.3). Hemorrhagic manifestations and sequelae of HIE in the premature infant readily detected by US include germinal matrix hemorrhage (GMH grades I–IV), intraventricular hemorrhage (IVH), periventricular hemorrhagic infarction (a.k.a. grade IV), and posthemorrhagic hydrocephalus [1–13,25] (Figs. 18.21, 18.22). Choroid plexus hemorrhage and hemorrhagic infarction in the term infant are also easily demonstrated. Portable US may effectively delineate the potential hemorrhagic or ischemic sequelae of ECMO. Although CT has been more reliable, high-resolution US using transfontanel and transcranial approaches, including the mastoid view, may detect extracerebral hemorrhage (subdural and subarachnoid) and posterior fossa collections (cerebellar or subdural) [1–13,25]. Color Doppler US, MRA, and CTA are all able to identify and distinguish the types of Galenic malformations, and provide follow-up (Fig. 18.23). Angiography is more specifically directed to the definitive interventional or surgical management of these and other vascular anomalies. Real-time Doppler US provides intraprocedural guidance and monitoring. The long-term sequelae of intracranial hemorrhage are often better demonstrated by MRI than by CT (e.g., hydrocephalus, atrophy, encephalomalacia, porencephaly, calcification, hemosiderin).

Occlusive neurovascular disease and sequelae

Occlusive neurovascular disease in the fetus, newborn, and infant may be arterial or venous in origin, and typically results in focal or multifocal lesions within the distribution of the

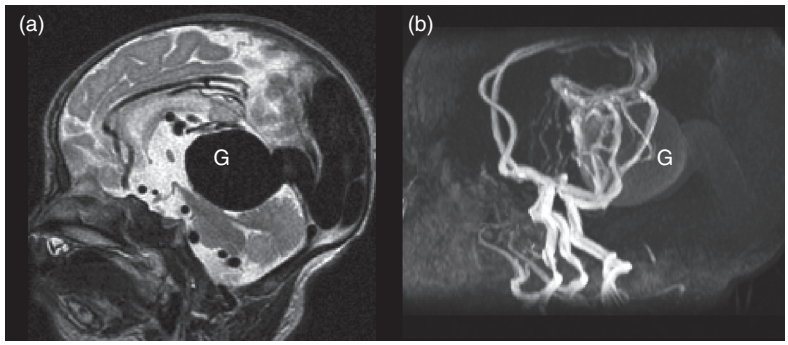

Fig. 18.23. Vein of Galen (G) vascular malformation (choroidal type) on (a) sagittal T2 and (b) lateral MRA.

Table 18.4. Occlusive neurovascular disease in the fetus, neonate, and infant

Idiopathic
Cardiac disease
Congenital
Acquired
Vascular maldevelopment
Atresia
Hypoplasia
Traumatic
Dissection
Vascular distortion
Air or fat emboli
Vasculopathy
Moyomoya
Fibromuscular dysplasia
Marfan syndrome
Takayasu arteritis
Kawasaki disease
Vasculitis
Polyarteritis nodosa
Lupus
Vasospasm
Migraine
Ergot poisoning
Subarachnoid hemorrhage
Drugs
Cocaine
Amphetamines
l-asparaginase
Oral contraceptives
Hypercoagulopathy (thrombophilias)
Protein S deficiency
Protein C deficiency
Antithrombin III deficiency
Factor V (Leiden) & prothrombin mutations
Antiphospholipid antibody (lupus, anticardiolipin)
Heparin cofactor II deficiency
Dehydration/hypernatremia
HIE/DIC
Sepsis/DIC
Polycythemia/hyperviscosity
Nephrotic syndrome
Oncologic disease
Hemolytic uremic syndrome
Hemoglobinopathies
Sickle cell disease
Infection
Meningoencephalitis
Sepsis
Metabolic disease
Homocystinuria
Dyslipoproteinemia
Fabry disease
Mitochondrial cytopathies
Familial lipid disorders
Other
Emboli from involuting fetal vasculature
Placental vascular anastomoses (twin gestation)
Co-twin fetal death
Fetofetal transfusion
ECMO
Catheterized vessel

Note:
See references [2–5,90].

occluded vessel or vessels [1–12] (Table 18.4). Arterial occlusive disease may be partial or complete, and may be due to embolization, thrombosis, or stenosis. The result may be ischemic infarction or hemorrhagic infarction followed by atrophy. Arterial occlusive disease may occur as a prenatal or perinatal event (emboli of placental origin, fetal heart, or involuting fetal vessels), as a complication of infection (e.g., meningitis), with congenital heart disease, or from a hypercoagulopathy (thrombophilias, prothrombotic disorders) [85–93]. The thrombophilias may be genetic or acquired,

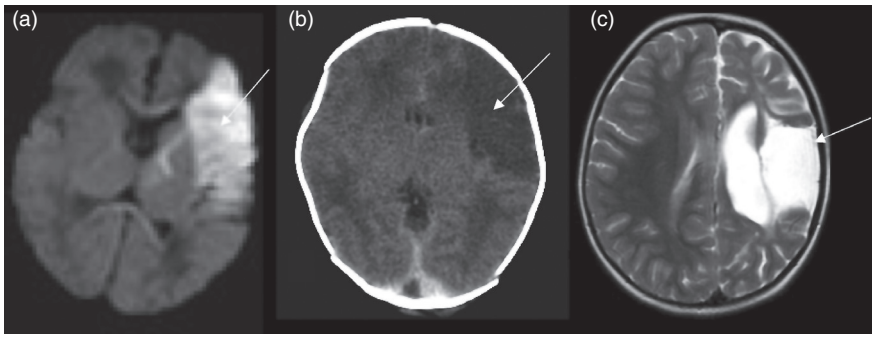

Fig. 18.24. Middle cerebal arterial infarction (arrows): (a) acute phase with edema on axial DWI; (b) subacute phase on CT; (c) chronic phase on axial T2 with hemiatrophy.

and include protein C and S deficiencies, activated protein C resistance, antiphospholipid antibody (lupus, anticardiolipin), antithrombin III deficiency, factor V Leiden, prothrombin gene mutation, methylene tetrahydrofolate reductase (MTHFR), homocysteine, factors VIII/IX/XI, anemia, polycythemia, and others. These are risk factors that are often provoked by "triggers" that may include acute systemic disease (e.g., dehydration, infection, trauma, hypoxia–ischemia) and chronic systemic disease (e.g., hematologic disorders, connective tissue disorders, lupus) [90]. Other causes include trauma (e.g., dissection), arteriopathies (e.g., moyamoya), and metabolic disorders (e.g., mitochondrial cytopathies). Conditions commonly associated with cortical or dural venous sinus occlusive disease include infection, dehydration, perinatal encephalopathy, cyanotic congenital heart disease, polycythemia, other hypercoagulable states, DIC, and trauma [1–12,85–94]. Color Doppler US may be used as a non-invasive tool for initial identification and monitoring of these infants. MRI is more sensitive and specific than US or CT for ischemic infarction, hemorrhagic infarction, and venous thrombosis [2–5,7,12,30,88,90] (Figs. 18.24, 18.25). MRA or CTA may also contribute to the diagnosis of arterial or venous occlusion and clarify (or obviate) the need for cerebral angiography, particularly when anticoagulation or thrombolysis is being considered. As mentioned earlier, PMRI, DWI, and MRS are contributing to the early diagnosis and timely treatment of ischemic insults. The long-term sequelae of infarction include atrophy, encephalomalacia, gliosis, mineralization, and porencephaly. These may be better shown by MRI than by CT.

Acute myelopathy due to HIE, vascular occlusion, hemorrhage, or vascular malformation is extremely rare in the perinatal period. Spinal MRI is the definitive procedure to evaluate spinal cord infarction or hemorrhage (see section on trauma, below). Spinal angiography is necessary to evaluate for vascular malformation in anticipation of interventional or surgical therapy [2,4].

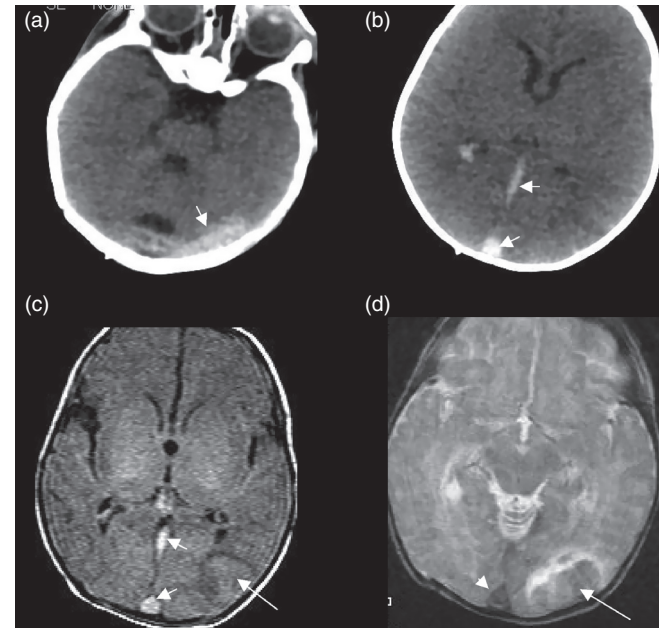

Fig. 18.25. Venous thromboses (short arrows) with hemorrhages and infarctions (long arrows) on (a,b) axial CT, (c) axial T1, (d) axial GRE in infant with hypercoagulable state.

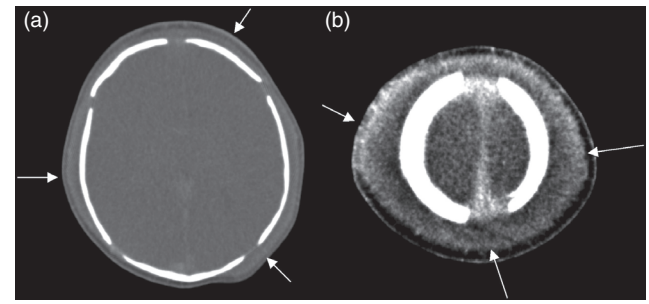

Fig. 18.26. Large bilateral subgaleal hematomas (arrows) on CT with (a) bone and (b) soft tissue algorithms.

Trauma

With improvements in resolution and the use of additional views (e.g., mastoid view), US may be used as the primary modality for evaluating the newborn with parturitional trauma. CT, however, is usually relied upon for delineating skull and scalp injury (e.g., subgaleal hematoma: Fig. 18.26), extracerebral hemorrhage (e.g., subarachnoid or subdural), posterior fossa hemorrhage, and direct (e.g., contusion, shear) versus indirect (e.g., HIE) brain injury [1–12,29,94–100]. CT is sufficiently sensitive and specific for acute hemorrhage and the complications or sequelae of fractures (e.g., depression, growing fracture, leptomeningeal cyst) (Fig. 18.27). Occasionally, skull films will demonstrate a skull fracture not shown by CT. It may occasionally be difficult to distinguish fracture

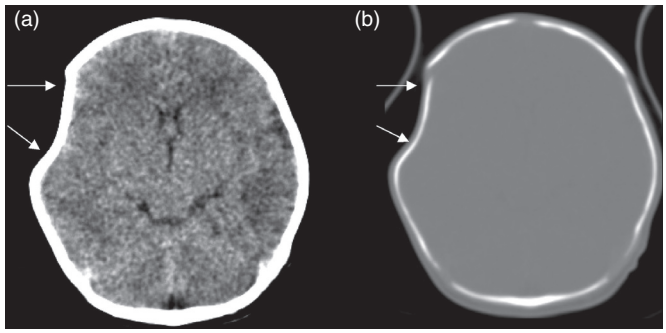

Fig. 18.27. Right frontal cranial depression (arrows) on CT with (a) soft tissue and (b) bone algorithms.

from sutures, synchondroses, and their variants or anomalies (e.g., fissures, accessory sutures, intrasutural bones). MDCT with 3D surface reconstructions may possibly be needed. MRI is probably necessary when neurologic deficits are present and the CT is negative or non-specific. In this situation MRI may reveal lesions such as brainstem infarction, traumatic axonal (shear) injury, and cortical contusion, or sequelae such as gliosis, microcystic encephalomalacia, and hemosiderin deposition. MRI is often more specific than CT for hemorrhage beyond the hyperacute/acute stage (Table 18.3). Color Doppler US, contrast-enhanced CT, or MRI may distinguish external hydrocephalus (dilated subarachnoid spaces) from chronic subdural hematomas (e.g., child abuse and its mimics) when non-enhanced CT demonstrates non-specific extracerebral collections [29]. Furthermore, hemosiderin as demonstrated by MRI is confirmation of a previous hemorrhage. In children with atypical intracranial hemorrhage on CT (e.g., hemorrhage out of proportion to the history of trauma, hemorrhage of varying age), MRI may show an existing vascular malformation, a hemorrhagic neoplasm, or other findings indicating the need for distinguishing child abuse from its mimics [29].

Initial evaluation of spine trauma (e.g., fracture/dislocation) may include plain films or US, but MDCT (including 2D reformatting and 3D surface reconstructions) is preferred. Abnormality on preliminary imaging, changing clinical signs, or unexplained brain injury may provide the indication for spinal MRI [2,4,29], including a STIR sequence. An existing spinal anomaly or mass should be ruled out. MRI is the procedure of choice to fully evaluate acute spinal injury (e.g., intraspinal hemorrhage, cord contusion, cord edema, transection, brachial plexus injury, ligamentous injury), and the sequelae of spinal injury (e.g., hydrosyringomyelia, cystic myelopathy, myelomalacia).

Infections and inflammatory processes

US or CT is often initially used to delineate CNS infection and its sequelae or complications. However, MRI is clearly superior for early detection, including the use of diffusion imaging, and for demonstrating the precise nature and extent of involvement using T2, FLAIR, GRE, and gadolinium-enhanced sequences (e.g., CMV) [1–12,101–103]. This includes meningoencephalitis due to TORCH infections (i.e., toxoplasmosis, other [e.g., syphilis], rubella, cytomegalovirus [CMV], herpes simplex virus [HSV2], human immunodeficiency virus [HIV]), and neonatal meningitis (e.g., Group B *Streptococcus, Listeria*, Gram-negative) (Figs. 18.28–18.33). Less common but increasingly prevalent causes of subacute and chronic CNS inflammation are the granulomatous meningoencephalitic infections (e.g., tuberculosis, spirochete, fungal, parasitic), particularly in immunocompromised hosts. The imaging pattern is often asymmetric and progressive. Such findings may include subarachnoid exudate, ventriculitis, edema, cerebritis, infarction, hydrocephalus, effusion, empyema, abscess, and in the chronic phase cystic encephalomalacia, atrophy, gliosis, and calcification.

Recurrent infectious or non-infectious CNS infection (e.g., meningitis) may require investigation for a "parameningeal focus" (e.g., sinus or mastoid infection, dermal sinus, primitive neurenteric connection, CSF leak after trauma, dermoid–epidermoid) [1–12]. Brain abscess or empyema may be associated with Gram-negative meningitis (e.g., *Citrobacter*) in the neonate. Suppurative collections related to sinus infection, trauma, surgery, sepsis, the immunocompromised state, or uncorrected cyanotic congenital heart disease primarily occur in older children. MRI is the imaging modality of choice for definitive evaluation and follow-up. Multiplanar T2, FLAIR, GRE, and DWI sequences are often necessary, along with gadolinium-enhanced T1 images, in order to delineate collections requiring drainage. Contrast-enhanced stereotactic MRI or CT and intraoperative US may provide additional guidance for surgery.

Plain films or SPECT have been used in the past for screening of suspected spinal-column infection (discitis, osteomyelitis) [2,5]. MRI, however, is now preferred for definitive diagnosis, treatment planning, and follow-up. CT may further assist in the delineation of bony involvement. MRI is also the procedure of choice for evaluating spinal neuraxis infection. STIR sequences and fat-suppressed gadolinium-enhanced techniques are particularly important for demonstrating suppurative collections (e.g., epidural abscess).

Metabolic, toxic, and neurodegenerative disorders

In the evaluation of neonatal encephalopathy and developmental delay (e.g., static encephalopathy vs. progressive encephalopathy), MRI is the only modality that can provide an accurate assessment of brain maturation based on myelination and cortical development [2–5,7,8,12,30,38,39,104–107] (Figs. 18.1–18.4). The clinical hallmark of a metabolic, toxic, or neurodegenerative disorder is "progressive" neurologic impairment in the absence of another readily identifiable process. These are to be distinguished from the "non-progressive" encephalopathies, for example, due to maldevelopment, hypoxia–ischemia, or infection. These disorders may be exogenous and internal (e.g., hypoglycemia, hyperbilirubinemia) or external (e.g., fetal alcohol syndrome). The endogenous disorders (e.g., inborn errors of metabolism) are not as

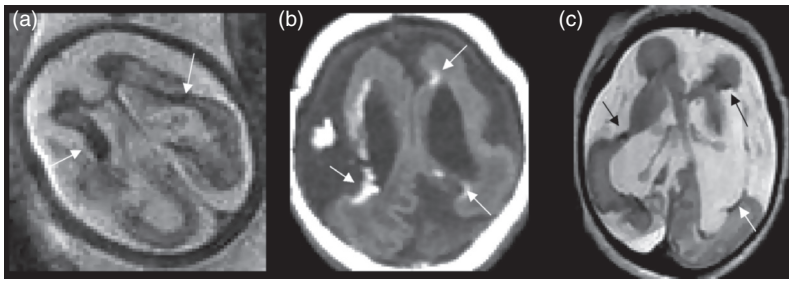

Fig. 18.28. Congential CMV on (a) fetal T2 and (b) neonatal T1 + (c) GRE MRI including dysplastic (microcephaly, undergyration) and encephaloclastic (cavitations) components plus T1 hyperintense/T2 hypointense mineralization (arrows).

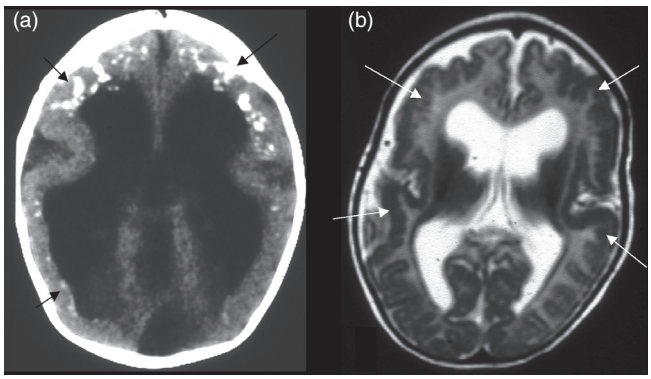

Fig. 18.29. Congenital CMV: (a) calcification (arrows) on CT; (b) diffuse polymicrogyria (arrows) on axial T2 MRI.

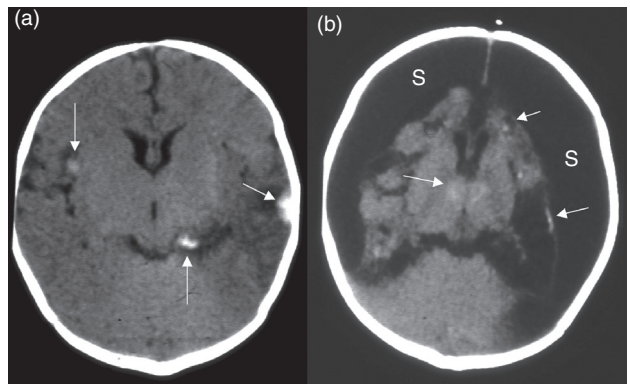

Fig. 18.32. HSV2 encephalitis on CT: (a) subacute phase, including hemorrhages (arrows); (b) chronic phase, with encephalomalacia, subdural collections (s), and calcifications (arrows).

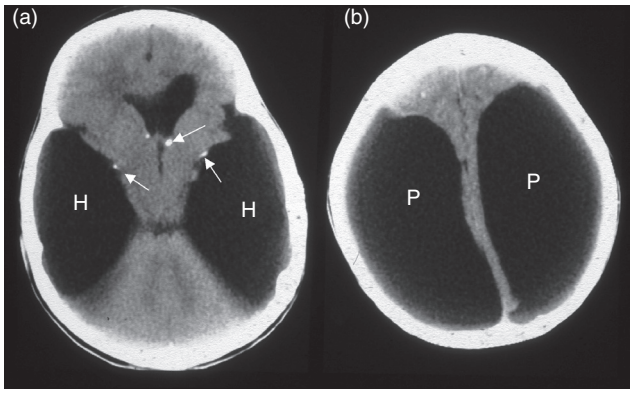

Fig. 18.30. Congenital toxoplasmosis: (a,b) CT with hydrocephalus (H), porencephaly (P), and calcifications (arrows).

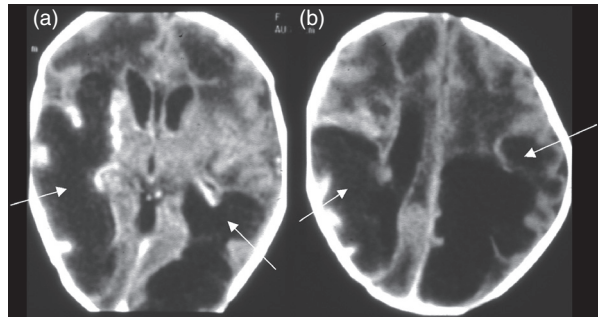

Fig. 18.33. *Citrobacter* meningitis: (a,b) CT with contrast-enhancing abscesses (arrows), ventriculitis, and hydrocephalus.

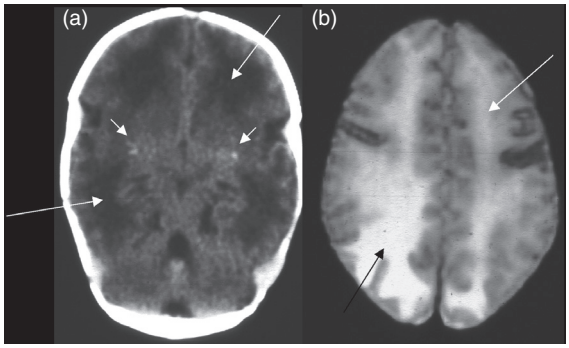

Fig. 18.31. Congenital rubella on (a) CT and (b) T2 MRI, including calcifications (short arrows) and leukoencephalitis (long arrows) with white-matter low densities and T2 high intensities.

rare as previously considered, and some are specifically treatable. Many are genetic and heredofamilial disorders such that genetic counseling and prenatal screening are important. Metabolic disorders may be classified in a number of ways including anatomic predilection (e.g., gray matter, white matter, both) and metabolic defect. Diagnosis is primarily a clinical one and may involve metabolic testing, genetic evaluation, or biopsy of CNS or extra-CNS tissues. MRI is superior to US and CT in evaluating disease extent and anatomic distribution. Occasionally MRI may demonstrate characteristic imaging findings (e.g., kernicterus, Zellweger disease). MRS contributes to the specific metabolic characterization of these disorders [39]. Stereotactic CT or MRI may serve as a guide for biopsy.

The classification of metabolic diseases may be biochemical, molecular, genetic, pathological, or clinical [2–5,7,8,12, 30,38,39,104–113] (Table 18.5). These disorders are often

Table 18.5. Metabolic, toxic, and neurodegenerative disorders

- Lysosomal disorders
  - *Lipidoses*
    - Fabry, Gaucher's and Niemann–Pick disease
    - GM_1 gangliosidosis
    - GM_2 gangliosidosis (Tay–Sachs and Sandhoff diseases)
    - Neuronal ceroid lipofuscinosis
  - *Mucopolysaccharidoses (MPS)*
    - Hurler, Scheie, Hurler–Scheie
    - Hunter
    - Sanfilippo A–D
    - Morquio A & B
    - Matoreaux-Lamy
    - Sly
  - *Mucolipidoses*
    - Mannosidosis, Fucosidosis, Sialidosis
  - *Lysosomal leukodystrophies*
    - Metachromatic leukodystrophy
    - Globoid cell leukodystrophy (Krabbe)
- Peroxisomal disorders
  - Adrenoleukodystrophy complex
  - Neonatal leukodystrophy
  - Zellweger syndrome
  - Infantile Refsum's syndrome
  - Rhizomelic chondrodysplasia punctata
  - Hyperpipecolic acidemia
  - Cerebrotendinous xanthomatosis
- Other leukodystrophies
  - Pelizaeus–Merzbacher disease
  - Canavan's disease
  - Alexander's disease
  - Cockayne's syndrome
  - Leukodystrophy with calcifications
- Mitochondrial (respiratory oxidative) disorders
  - Leigh's disease
  - Kearns–Sayre syndrome
  - MELAS syndrome
  - MERRF syndrome
  - Alper's syndrome (poliodystrophy)
  - Menkes' disease (trichopoliodystrophy)
  - Marinesco-Sjogren syndrome
  - Infantile bilateral striatal necrosis
  - Lebers hereditary optic atrophy
  - L-Carnitine deficiency
- Amino acid disorders
  - Phenylketonuria
  - Homocystinuria
  - Non-ketotic hyperglycinemia
  - Maple syrup urine disease
  - Glutaric aciduria, type I
  - Glutaric aciduria, type II
  - Methylmalonic and propionic acidurias
  - Urea cycle defects (e.g., OTC deficiency)
  - Oculocerebrorenal syndrome
  - Pyridoxine dependency
- Carbohydrate and other storage disorders
  - Galactosemia
  - Glycogen storage diseases (i.e. Pompe)
  - Carbohydrate-deficient glycoprotein syndrome
  - Niemann-Pick
  - Gaucher
  - Farber
  - Infantile sialidosis
- Liver metabolic disorders
  - Wilson's disease (hepatolenticular degeneration)
  - PKAN
  - Hyperbilirubinemia (see toxic encephalopathies)
  - Hepatocerebral syndromes (see toxic encephalopathies)
- Diseases of the cerebellum, brainstem, and spinal cord
  - Friedreich's ataxia
  - Olivopontocerebellar atrophies
  - Ataxia–telangiectasia
  - Carbohydrate-deficient glycoprotein syndrome
  - Infantile neuraxonal dystrophy
- Other metabolic and neurodegenerative diseases
  - Juvenile multiple sclerosis
  - Molybdenum cofactor deficiency
  - 3-Hydroxy-3-methylglutaryl-coenzyme A lyase deficiency
  - Idiopathic leukoencephalopathy
- Diseases of the basal ganglia
  - Sulfite oxidase deficiency
  - Parathyroid disease
  - Tuberous sclerosis
  - Down's syndrome
  - Progressive encephalopathy with basal ganglia calcifications and CSF lymphocytosis
  - Inflammatory, toxic, and anoxic conditions
  - Radiation therapy
  - Renal tubular acidosis and osteoporosis
  - Huntington's disease
  - Fahr's disease
  - PKAN
  - Cockayne
  - Wilson
- Toxic encephalopathies
  - Exogenous internal toxicities
    - Hyperbilirubinemia
    - Hepatocerebral syndromes
    - Hypoglycemia
    - Hypothermia and hyperthermia
    - Paraneoplastic toxins
    - Hemolytic uremic syndrome
    - Uremia
    - Ion imbalance disorders
    - Endocrinopathies
    - Porphyria
  - Exogenous external toxicities
    - *Vitamin deficiencies/depletions*
      - Vitamin B_1
      - Folate
      - Vitamin B_{12}
      - Biotin
      - Vitamin K
      - Vitamin C
      - Vitamin D
    - *Toxins*
      - Mercury poisoning
      - Methanol
      - Toluene
      - Carbon monoxide
      - Cyanides and sulfides
      - Lead
      - Alcohol
      - Cocaine and heroin
    - *Anticonvulsants*
    - *Drug-induced*
      - Methotrexate
      - Cyclosporine
      - Tacrolimus
      - Carmustine, cytosine arabiniside

Note:
See references [2,4,5,106,107].

categorized according to the metabolic defect. Such a classification includes the lysosomal disorders (e.g., Krabbe), peroxisomal defects (e.g., Zellweger), the mitochondrial disorders (e.g., Leigh, Menkes), organic and aminoacidopathies (e.g., nonketotic hyperglycinemia), disorders of carbohydrate metabolism (e.g., glycogen storage disease), liver metabolic disorders, and miscellaneous. Certain clinical features that assist in directing the initial evaluation of these patients may also provide a basis for classification (e.g., macrocephaly in maple syrup urine disease). The ideal radiological classification would categorize the diseases by the anatomic distribution of the pathological process using CT and MRI. Unfortunately, most of these conditions affect multiple sites, and considerable overlap in appearance is found. However, a practical imaging classification may be based on the predominant areas of involvement including the white matter (subcortical, periventricular), gray matter (cortical, deep), basal ganglia, brainstem, cerebellum, spinal cord, and peripheral nervous system [2,5,12,7,8,12,39, 104–107].

Disorders primarily affecting cortical gray matter

Endogenous metabolic disorders which primarily, or predominantly, affect the cortical gray matter include the storage diseases that result from lysosomal enzyme defects [2,5,39,107]. However, these findings are often non-specific, and the differential diagnosis may include diffuse cortical atrophy due to any number of causes. Other considerations include the end stage of a static encephalopathy (e.g., post-HIE or post-infection), or "atrophy" related to chronic systemic disease, malnutrition, or certain types of therapy (e.g., steroids).

Disorders primarily affecting deep gray matter

Metabolic disorders may primarily involve the deep gray matter (including mineralization) [2,5,39,107,110–113]. Those disorders primarily involving the corpus striatum (i.e., caudate and putamen) include the mitochondrial disorders, organic and aminoacidopathies, juvenile Huntington's disease, Wilson disease, and Cockayne's syndrome. Those disorders primarily involving the globus pallidus include the aminoacidopathies, hyperbilirubinemia, pentothenate kinase associated neurodegeneration (PKAN, formerly Hallervorden–Spatz disease), and toxic exposure (e.g., carbon dioxide) (Figs. 18.34, 18.35). It is unusual to see isolated involvement of the thalami in any of the metabolic disorders. However, thalamic involvement may be an early or dominant feature of Krabbe disease or GM2 gangliosidosis. It may also be seen in the infantile form of Leigh disease along with extensive brainstem, basal ganglia, and cerebral white-matter involvement. In general, the differential diagnosis, depending on the clinical picture and timing of the imaging, may also include profound HIE, hypoglycemia, toxic exposure (e.g., methane, cyanide), osmolar myelinolysis, striatal necrosis, and meningoencephalitis.

Disorders primarily affecting white matter

Those disorders which primarily, or predominantly, affect the white matter are known as the leukoencephalopathies [2,5,39,107–109]. Traditionally, leukoencephalopathies have been divided into dysmyelinating and myelinoclastic disorders. In dysmyelinating disorders an intrinsic (inherited) enzyme deficiency results in the disturbed formation, destruction, or turnover of the essential components of myelin. They are also referred to as the leukodystrophies. The pattern of damage is symmetrical in both hemispheres, has diffuse margins, often spares the arcuate fibers, and consistently involves the cerebellar white matter. The leukodystrophies are primarily associated with the lysosomal and peroxisomal disorders (e.g., metachromatic leukodystrophy, Krabbe leukodystrophy, and the adrenoleukodystrophy complex [ALD]), and with diseases of white matter (e.g., Pelizaeus–Merzbacher, Canavan, Alexander, and Cockayne). Included in the differential diagnosis is infantile-onset leukoencephalopathy with swelling (macrocephaly) and mild clinical course. Early central white-matter involvement may suggest Krabbe (also, abnormal thalami), ALD, phenylketonuria, maple syrup urine disease (MSUD: Fig. 18.34), or Lowe syndrome. The lack of myelination

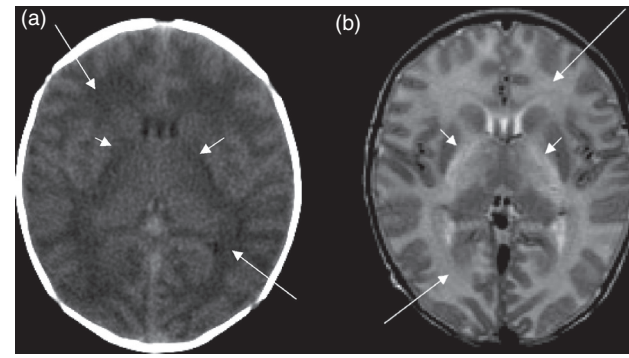

Fig. 18.34. Maple syrup urine disease in neonate with globus pallidus (short arrows) and white matter (long arrows) edema on (a) axial CT and (b) axial T2 MRI.

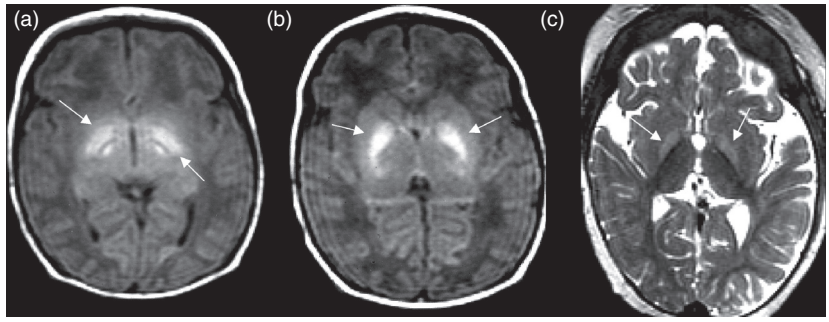

Fig. 18.35. Bilirubin encephalopathy and kernicterus on MRI with (a,b) globus pallidus and subthalamic T1 hyperintensity (arrows) in subacute phase, and (c) T2 hyperintensity (arrows) plus atrophy in chronic phase.

(hypomyelination) may suggest Pelizaeus–Merzbacher disease or Menkes' disease. In myelinoclastic disorders, the myelin sheath is intrinsically normal until it yields to exogenous or endogenous myelinotoxic factors. The pattern of damage is asymmetric, is sharply demarcated, irregularly involves the subcortical arcuate fibers, and may spare the cerebellum. Examples are the infectious and postinfectious demyelinating diseases (e.g., TORCH, HIV, SSPE, ADEM) and the vasculitides (e.g., lupus). Non-specific white-matter abnormalities may be seen with a variety of metabolic, neurodegenerative, infectious, postinfectious, toxic, and vascular processes. In this situation, the clinical findings must be relied upon. An important example is posterior reversible leukoencephalopathy (e.g., hypertension, transplant, cyclosporine, renal disease). Also, it is important to remember that the most common causes of cerebral white-matter abnormalities (particularly periventricular) and prominent Virchow–Robin spaces in children with developmental delay are the static leukoencephalopathies (e.g., maldevelopmental, undermyelination, postinflammatory, postischemic, idiopathic).

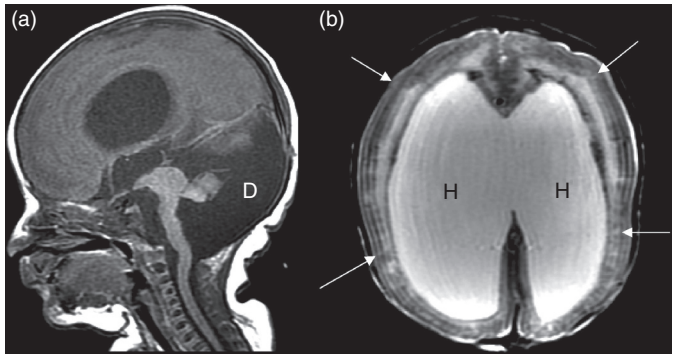

Fig. 18.36. Walker–Warburg with Dandy–Walker malformation (D) on (a) sagittal T1 plus (b) cobblestone lissencephaly (arrows) with extensive white-matter dysplasia and hydrocephalus (H) on axial T2 MRI.

Disorders affecting both white matter and cortical gray matter

A number of metabolic disorders involve both gray and white matter [2,5,39,107–109]. Those disorders associated with cortical atrophy along with white-matter involvement include lysosomal disorders such as the lipidoses and mucopolysaccharidoses (also, associated skeletal dysplasia), and mitochondrial disorders such as Alper disease and Menkes' disease. If there is a diffuse cortical dysgenesis (e.g., lissencephaly, polymicrogyria) associated with white-matter abnormalities, then peroxisomal disorders such as Zellweger syndrome should be considered along with congenital infections (e.g., cytomegaloviral), and the congenital muscular dystrophies (e.g., Fukuyama, Walker–Warburg, Santavuori) (Fig. 18.36).

In hypoglycemia, there is predominant involvement of the parieto-occipital gray and white matter, and especially the primary visual cortex (Fig. 18.37). This pattern is to be distinguished from a predominant posterior border-zone HIE and from dural venous sinus thrombosis primarily in the distribution of the straight sinus, posterior superior sagittal sinus, and/or the inferior sagittal sinus.

Disorders affecting both white matter and deep gray matter

Disorders associated with deep gray-matter involvement, in addition to white-matter abnormalities, include those with primarily corpus striatum involvement (Leigh [Fig. 18.38], MELAS, Wilson's, Cockayne), those with predominant thalamic abnormalities (Krabbe, GM2 gangliosidoses), and those with primarily globus pallidus involvement (Canavan, MSUD, methylmalonic/propionic acidopathy, Kearns–Sayre) [2,5,39,107–113]. Sulfite oxidase deficiency also involves the basal ganglia and white matter and can mimic HIE [114] (Fig. 18.39). Included in

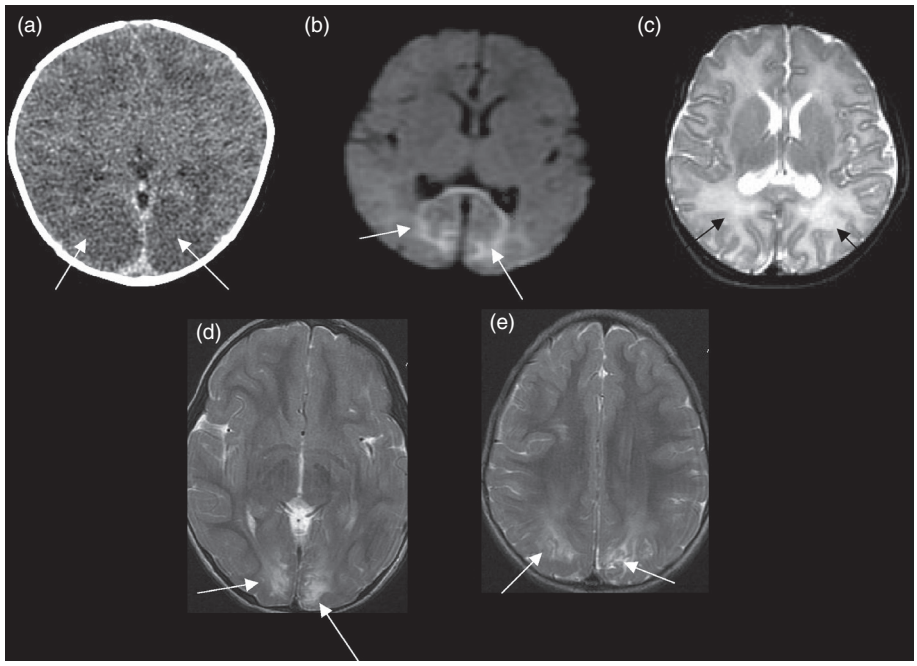

Fig. 18.37. Hypoglycemia with parieto-occipital involvement (arrows) in the subacute phase with edema as (a) low density on CT, and as high intensity on (b) DWI and (c) T2 MRI; also (d,e) the chronic phase with atrophy and gliosis on T2 MRI.

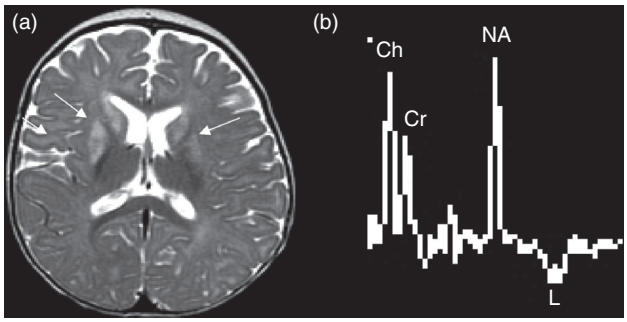

Fig. 18.38. Leigh syndrome with basal-ganglia lesions (arrows) and white-matter involvement: (a) axial T2 MRI; (b) lactate doublet (L) on MRS.

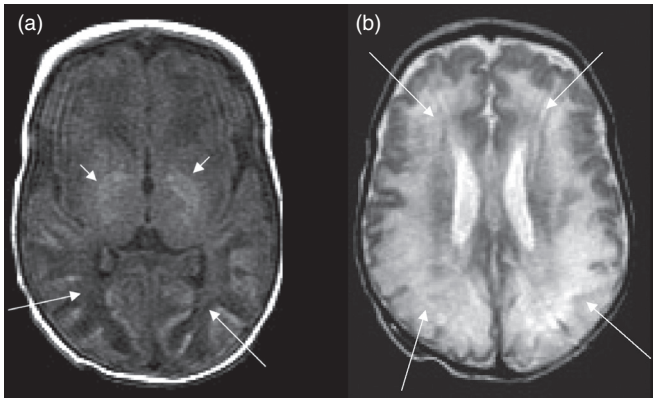

Fig. 18.39. Sulfite oxidase deficiency with thalamic (short arrows) and diffuse white-matter involvement (long arrows) on (a) axial T1 and (b) T2 MRI.

the differential diagnoses, depending on the clinical context, are profound HIE, osmolar myelinolysis, bilirubin encephalopathy (kernicterus), toxic exposure, and infectious or postinfectious processes (e.g., TORCH, HIV, ADEM).

MR spectroscopy (MRS) in metabolic disorders

Proton (hydrogen-1) MRS using both short and long TE acquisitions (e.g., TEs 35, 144) is being increasingly used clinically to evaluate brain development and maturation, as well as patients with metabolic and other disorders [12,38,39]. The normal MR brain spectra show an evolution from the immature infantile pattern (e.g., decreased *N*-acetyl-aspartate [NAA] relative to choline [Ch]) to the mature, adult pattern (e.g., increased NAA to Ch) (Fig. 18.3). Although many of the metabolic and neurodegenerative disorders have specific biochemical markers, most of the disorders have no differentiating features. Non-specific MRS abnormalities are those that reflect brain destruction and reactive changes including delayed maturation, neuronal loss, axonal degeneration, demyelination, and gliosis. Alterations in metabolites are often displayed as a ratio relative to the reference metabolite, creatine (Cr), an energy marker. In disorders in which there is predominant neuronal degeneration (i.e., loss of cell bodies, axons) and atrophy, or oligodendroglial loss, the major MRS finding is a decrease in *N*-acetyl-aspartate (NAA), a neuronal (neurons including axons) and immature oligodendroglial marker. In disorders in which there is predominant loss of myelin sheaths with secondary axonal degeneration and gliosis (e.g., demyelination), the characteristic spectral abnormalities are characterized by elevated lipids, a marker for myelin destruction; elevated choline (Ch), a marker of membrane turnover (e.g., myelin, glial); variable increases in lactate (L), a marker of anaerobic glycolysis; elevated glutamate/glutamine (Glx), neuroexcitatory amino acid markers; and elevated myoinositols (mI), also an osmolyte and glial marker. Associated neuronal (e.g., axonal) or oligodendroglial damage is indicated by a decrease in NAA.

More specific MRS abnormalities may be seen in a number of disorders [39]. Abnormal MRS spectra have been reported with some of the lysosomal defects such as Niemann–Pick disease (abnormal lipid peak at 1.2 ppm), the mucopolysaccharidoses (decreased NAA late), and metachromatic leukodystrophy (decreased NAA, Ch, and Cr; increased mI and L). MRS abnormalities have been observed with a number of the peroxisomal disorders including adrenoleukodystrophy (decreased NAA with increased Ch, Glx, mI, lipids, and L) and Zellweger syndrome (decreased NAA with increased lipids and Glx). Other leukodystrophies associated with observed MRS findings are Canavan disease (increased NAA with decreased Ch and Cr plus increased mI and L), Alexander disease (decreased NAA with increased L), and Pelizaeus–Merzbacher disease (normal early; decreased NAA and increased Ch late). Primary and secondary disorders of energy metabolism have been associated with MRS findings of decreased NAA and increased L, including mitochondrial disorders such as Leigh disease and MELAS (Fig. 18.38). Similar findings, however, are present with acute/subacute hypoxia–ischemia (plus elevated Glx, decreased Cr, and increased lipids) (Fig. 18.18). Aminoacidopathies with reportedly abnormal spectra include phenylketonuria (increased phenylalanine peak at 7.37 ppm), maple syrup urine disease (abnormal peak at 0.9 ppm), and non-ketotic hyperglycinemia (elevated glycine peak at 3.55 ppm). Other metabolic disorders associated with abnormal MRS findings include the creatine deficiencies (decreased, absent Cr), hepatic encephalopathy (increased Glx with decreased inositols and Ch), and hyperosmolar states (increased inositols, Cr, and Ch). Neoplastic processes characteristically show elevated Ch/Cr, decreased NAA/Cr, and decreased NAA/Cr ratios. Inflammatory processes may be differentiated from neoplastic and other processes by the suppressed mI peak [12].

Summary

US and CT may provide important screening information, particularly with regard to hemorrhage, trauma, hydrocephalus, infection, and gross macrostructural anomalies. However, current and advanced MRI techniques provide more definitive macrostructural, microstructural, and functional imaging information in both the early and late assessment of fetal and neonatal CNS injuries.

References

1. Blankenburg FG, Barnes PD. Structural and functional imaging of hypoxic–ischemic injury (HII) in the fetal and neonatal brain. In Stevenson D, Benitz W, Sunshine P, eds., *Fetal and Neonatal Brain Injury*, 3rd edn. Cambridge: Cambridge University Press, 2003: 446–89.
2. Barnes P. State of the art: neuroimaging and the timing of fetal and neonatal brain injury. *J Perinatol* 2001; **21**: 44–60.
3. Winkler P, Zimmerman RA. *Perinatal Brain Injury. Neuroimaging: Clinical and Physical Principles*. New York, NY: Springer, 2000: 531–83.
4. Barkovich A. *Pediatric Neuroimaging*, 4th edn. Philadelphia, PA: Lippincott-Raven, 2005: 190–290.
5. Volpe JJ. *Neurology of the Newborn*, 4th edn. Philadelphia, PA: Saunders, 2001.
6. Ment L, Bada H, Barnes P, *et al.* Practice parameter: neuroimaging of the neonate. *Neurology* 2002; **58**: 1726–38.
7. Ferriero D. Neonatal brain injury. *N Engl J Med* 2004; **351**: 1985–95.
8. Barkovich A. MR imaging of the neonatal brain. *Neuroimaging Clin N Am* 2006; **16**: 117–36.
9. Rutherford M, Srinivasan L, Dyet L, *et al.* MRI in perinatal brain injury. *Pediatr Radiol* 2006; **36**: 582–92.
10. Zimmerman R, Bilaniuk L. Neuroimaging evaluation of cerebral palsy. *Clin Perinatol* 2006; **33**: 517–44.
11. Triulzi F, Parazzini C, Righini A. Patterns of damage in the mature neonatal brain. *Pediatr Radiol* 2006; **36**: 608–20.
12. Panigrahy A, Blumel S. Advances in MR neuroimaging techniques in the evaluation of neonatal encephalopathy. *Top Magn Reson Imaging* 2007; **18**: 3–30.
13. Barnes PD, Taylor GA. Imaging of the neonatal central nervous system. *Neurosurgery Clin North Am* 1998; **1**: 17–48.
14. Allison JW, Seibert JJ. Transcranial Doppler in the newborn with asphyxia. *Neuroimaging Clin N Am* 1999; **9**: 11–16.
15. Blankenberg FG, Loh N, Bracci P, *et al.* Sonography, CT, and MR imaging: a prospective comparison of neonates with suspected intracranial ischemia and hemorrhage. *AJNR Am J Neuroradiol* 2000; **21**: 213–18.
16. Debillon T, N'Guyen, Muet A, *et al.* Limitations of ultrasonography for diagnosing white matter damage in preterm infants. *Arch Dis Child Fetal Neonatal Ed* 2003; **88**: F275–9.
17. Laptook A, O'Shea M, Shankaran S, *et al.* Adverse neurodevelopmental outcomes among extremely low birth weight infants with normal head ultrasound. *Pediatrics* 2005; **115**: 673–80.
18. Pinto-Martin JA, Riolo S, Cnaan A, *et al.* Cranial ultrasound prediction of disabling and nondisabling cerebral palsy at age two in a low birthweight population. *Pediatrics* 1995; **95**: 249–54.
19. Maalouf EF, Duggan PJ, Counsell SJ, *et al.* Comparison of findings on cranial ultrasound and magnetic resonance imaging in preterm neonates. *Pediatrics* 2001; **107**: 719–27.
20. Sie LT, van der Knapp MD, van Wezel-Meijler G, *et al.* Early MR features of hypoxic-ischemic brain injury in neonates with periventricular densities on sonograms. *AJNR Am J Neuroradiol* 2000; **21**: 852–61.
21. Childs AM, Cornette L, Romenghi LA, *et al.* Magnetic resonance and cranial ultrasound characteristics of periventricular white matter abnormalities in newborn infants. *Clin Radiol* 2001; **56**: 647–55.
22. Roelants-van Rijn AM, Groenendaal F, Beek FJ, *et al.* Parenchymal brain injury in the preterm infant: comparison of cranial ultrasound, MRI and neurodevelopmental outcome. *Neuropediatrics* 2001; **32**: 80–9.
23. Inder TE, Anderson NJ, Spencer C, *et al.* White matter injury in the premature infant: a comparison between serial cranial sonographic and MR findings at term. *AJNR Am J Neuroradiol* 2003; **24**: 805–9.
24. Miller SP, Cozzio C, Goldstein RB, *et al.* Comparing the diagnosis of white matter injury in premature newborns with serial MR imaging and transfontanel ultrasonography findings. *AJNR Am J Neuroradiol* 2003; **24**: 1661–9.
25. Hintz SR, Slovis T, Bulas D, *et al.* Interobserver reliability and accuracy of cranial ultrasound scanning interpretation in premature infants. *J Pediatr* 2007; **150**: 592–6.
26. Mirmiran M, Barnes P, Keller K, *et al.* Neonatal brain MRI before discharge is better than serial cranial ultrasound in predicting cerebral palsy in very low birth weight preterm infants. *Pediatrics* 2004; **114**: 992–8.
27. Slovis T. Children, computed tomography radiation dose, and the As Low As Reasonably Achievable (ALARA) concept. *Pediatrics* 2003; **112**: 971–2.
28. Vertinzksy A, Barnes P. Macrocephaly, increased intracranial pressure, and hydrocephalus in the infant and young child. *Top Magn Reson Imaging* 2007; **18**: 31–52.
29. Barnes P, Krasnokutsky M. Imaging of the CNS in suspected or alleged nonaccidental injury, including the mimics. *Top Magn Reson Imaging* 2007; **18**: 53–74.
30. Mukherjee P. Advanced pediatric imaging. *Neuroimaging Clin N Am* 2006; **16**(1).
31. Levine D, Barnes PD, Robertson RR, *et al.* Fast MR imaging of fetal central nervous system abnormalities. *Radiology* 2003; **229**: 51–61.
32. Garel C, Delezide A, Elmaleh-Berges M, *et al.* Contribution of fetal MRI in the evaluation of cerebral ischemic lesions. *AJNR Am J Neuroradiol* 2004; **25**: 1563–1568.
33. Levine D, Barnes P. MR imaging of fetal CNS abnormalities. In Levine D, ed., *Atlas of Fetal MRI*. Boca Raton, FL: Taylor & Francis Group, 2005: 25–72.
34. Griffiths P, Widjaja E, Paley M, *et al.* Imaging of the fetal spine in utero: diagnostic accuracy and impact on management. *Pediatr Radiol* 2006; **36**: 927–33.
35. Garel C. New advances in fetal MR neuroimaging. *Pediatr Radiol* 2006; **36**: 621–5.
36. Glenn O, Barkovich J. Magnetic resonance imaging of the fetal brain and spine. Part 1. *AJNR Am J Neuroradiol* 2006; **27**: 1604–11; Part 2. *AJNR Am J Neuroradiol* 2006; **27**: 1807–14.
37. Barkovich AJ, Baranski K, Vigneron D, *et al.* Proton MR spectroscopy in the evaluation of asphyxiated term neonates. *AJNR Am J Neuroradiol* 1999; **20**: 1399–405.
38. Vigneron DB. Magnetic resonance spectroscopic imaging of human brain development. *Neuroimag Clin N Am* 2006; **16**; 75–86.
39. Cecil K. MR spectroscopy of metabolic disorders. *Neuroimaging Clin N Am* 2006; **16**: 87–116.
40. Barkovich A, Miller S, Bartha A. MR imaging, MR spectroscopy, and diffusion tensor imaging of sequential studies in neonates with encephalopathy. *AJNR Am J Neuroradiol* 2006; **27**: 533–47.

41. Wang J, Licht D. Pediatric perfusion MRI using arterial spin labeling. *Neuroimaging Clin N Am* 2006; **16**: 149–68.
42. Huppi PS, Maier SE, Peled S, *et al.* Microstructural development of human newborn cerebral white matter assessed in vivo by diffusion tensor magnetic resonance imaging. *Pediatr Res* 1998; **44**: 584–90.
43. Neil JJ, Shiran SI, McKinstry RC. Normal brain in human newborns: apparent diffusion coefficient and diffusion anisotropy measured by using diffusion tensor MR imaging. *Radiology* 1998; **209**: 57–66.
44. Johnson AJ, Lee BCP, Lin W. Echoplanar diffusion-weighted imaging in neonates and infants with suspected hypoxic–ischemic injury. *AJNR Am J Neuroradiol* 1999; **172**: 219–26.
45. Robertson RL, Ben-Sira L, Barnes PD, *et al.* MR line scan diffusion imaging of term neonates with perinatal brain ischemia. *AJNR Am J Neuroradiol* 1999; **20**: 1658–70.
46. Phillips MD, Zimmerman RA. Diffusion imaging in pediatric hypoxic-ischemic injury. *Neuroimaging Clin N Am* 1999; **9**: 41–52.
47. Inder T, Huppi PS, Zientara GP, *et al.* Early detection of periventricular leukomalacia by diffusion-weighted magnetic resonance imaging techniques. *J Pediatr* 1999; **134**: 631–4.
48. Inder TE, Huppi PS, Warfield S, *et al.* Periventricular white matter injury in the premature infant followed by reduced cerebral cortical gray matter volume at term. *Ann Neurol* 1999; **46**: 755–60.
49. Huppi PS, Murphy B, Maier SE, *et al.* Microstructural brain development after perinatal cerebral white matter injury assessed by diffusion tensor MR imaging. *Pediatrics* 2001; **107**: 455–60.
50. Arzoumanian Y, Mirmiran M, Barnes P, *et al.* Diffusion tensor brain imaging findings at term-equivalent age may predict neurologic abnormalities in low birth weight preterm infants. *AJNR Am J Neuroradiol* 2003; **24**: 1646–53.
51. Counsell S, Allsop J, Harrison M, *et al.* Diffusion-weighted imaging of the brain in preterm infants with focal and diffuse white matter abnormality. *Pediatrics* 2003; **112**: 1–7.
52. Sagar P, Grant PE. Diffusion-weighted imaging: pediatric clinical applications. *Neuroimaging Clin N Am* 2006; **16**: 45–74.
53. Mukherjee P, McKinstry R. Diffusion tensor imaging and tractography of human brain development. *Neuroimaging Clin N Am* 2006; **16**: 19–44.
54. van der Knaap M, Valk J. Classification of congenital abnormalities of the CNS. *AJNR Am J Neuroradiol* 1988; **9**: 315–26.
55. Barkovich AJ, Truwit CL. Brain damage from perinatal asphyxia: correlation of MR findings with gestational age. *AJNR Am J Neuroradiol* 1990; **11**: 1087–96.
56. Aida N, Nishimura G, Hachiya Y, *et al.* MR imaging of perinatal brain damage: comparison of clinical outcome with initial follow-up MR findings. *AJNR Am J Neuroradiol* 1992; **19**: 1909–22.
57. Barkovich A, Hallam D. Neuroimaging in perinatal hypoxic–ischemic injury. *Ment Retard Dev Disabil Res Rev* 1997; **3**: 28–41.
58. Cowan F, Rutherford M, Groenendaal F, *et al.* Origin and timing of brain lesions in term infants with neonatal encephalopathy. *Lancet* 2003; **361**: 736–42.
59. Miller S, Ramaswamy V, Michelson D, *et al.* Patterns of brain injury in term neonatal encephalopathy. *J Pediatr* 2005; **146**: 453–60.
60. Lupton BA, Hill A, Roland EH, *et al.* Brain swelling in the asphyxiated term newborn: pathogenesis and outcome. *Pediatrics* 1988; **82**: 139–46.
61. Vannucci RC, Christensen MA, Jager JY. Nature, time-course, and extent of cerebral edema in perinatal hypoxic–ischemic brain damage. *Pediatr Neurol* 1993; **9**: 29–34.
62. Pinto-Martin JA, Riolo S, Cnaan A, *et al.* Cranial ultrasound prediction of disabling and nondisabling cerebral palsy at age two in a low birthweight population. *Pediatrics* 1995; **95**: 249–54.
63. Goetz MC, Gretebeck RJ, Oh KS, *et al.* Incidence, timing and follow-up of periventricular leukomalacia. *Am J Perinatol* 1995; **12**: 325–7.
64. Valkama AM, Pääkkö ELE, Vainionpää LK, *et al.* Magnetic resonance imaging at term and neuromotor outcome in preterm infants. *Acta Paediatr* 2000; **89**: 348–55.
65. Perlman JM, Rollins N. Surveillance protocol for the detection of intracranial abnormalities in premature neonates. *Arch Pediatr Adolesc Med* 2000; **154**: 822–6.
66. Volpe JJ. Neurobiology of periventricular leukomalacia in the premature infant. *Pediatr Res* 2001; **50**: 553–62.
67. Panigrahy A, Barnes PD, Robertson RL, *et al.* Volumetric brain differences in children with periventricular T2-signal hyperintensities: a grouping by gestational age at birth. *AJR Am J Roentgenol* 2001; **177**: 695–702.
68. Miller SP, Hoque NN, Piecuch RE, *et al.* The spectrum of cerebellar hemorrhage in premature newborns. *Pediatr Res* 2003; **53**: 537A (abst #3040).
69. Austin NC, Woodward L, Spencer C, *et al.* Neurodevelopmental outcome at one year in a regional cohort of very low birth weight infants: correlation with MRI at term. *Pediatr Res* 2003; **53**: 398A (abst #2253).
70. Volpe JJ. Cerebral white matter injury of the premature infant: more common than you think. *Pediatrics* 2003; **112**: 176–80.
71. Inder TE, Wells SJ, Mogridge NB, *et al.* Defining the nature of the cerebral abnormalities in the premature infant: a qualitative magnetic resonance imaging study. *J Pediatr* 2003; **143**: 171–9.
72. Panigrahy A, Barnes PD, Robertson RL, *et al.* Quantitative analysis of the corpus callosum in children with cerebral palsy and developmental delay: correlation with cerebral white matter volume. *Pediatr Radiol* 2005; **35**: 1199–207.
73. Bodensteiner J, Johnsen S. MRI findings in children surviving extremely premature delivery and extremely low birthweight with cerebral palsy. *J Child Neurol* 2006; **21**: 743–7.
74. Dyet L, Kennea N, Counsell S, *et al.* Natural history of brain lesions in extremely preterm infants studied with serial MRI from birth and neurodevelopmental assessment *Pediatrics* 2006; **118**: 536–48.
75. Khwaja O, Volpe J. Pathogenesis of cerebral white matter injury of prematurity. *Arch Dis Child Fetal Neonatal Ed* 2008; **93**: F153–61.
76. Barkovich AJ. MR and CT evaluation of profound neonatal and infantile asphyxia. *AJNR Am J Neuroradiol* 1992; **13**: 959–72.
77. Barkovich AJ, Sargent SK. Profound asphyxia in the premature infant: imaging findings. *AJNR Am J Neuroradiol* 1995; **16**: 1837–46.
78. Barkovich AJ, Westmark K, Partridge C, *et al.* Perinatal asphyxia: MR findings in

the first 10 days. *AJNR Am J Neuroradiol* 1995; **16**: 427–39.

79. Roland EH, Poskitt K, *et al.* Perinatal hypoxic–ischemic thalamic injury: clinical features and neuroimaging. *Ann Neurol* 1998; **44**: 161–6.
80. Sargent M, Poskitt K, Roland E, *et al.* Cerebellar vermian atrophy after neonatal hypoxic–ischemic encephalopathy. *AJNR Am J Neuroradiol* 2004; **25**: 1008–15.
81. Boichot C, Walker P, Durand C, *et al.* Term neonate prognosis after perinatal asphyxia: contributions of MR imaging, MR spectroscopy, relaxation times, and ADCs. *Radiology* 2006; **239**: 839–48.
82. Shankaran S, Laptook A, Ehrenkranz R, *et al.* Whole-body hypothermia for neonates with hypoxic–ischemic encephalopathy. *N Engl J Med* 2005; **353**: 1574–84.
83. Bulas D, Glass P. Neonatal ECMO: neuroimaging and neurodevelopmental outcome. *Semin Perinatol* 2005; **29**: 58–65.
84. Zuerrer M, Martin E, Boltshauser E. MRI of intracranial hemorrhage in neonates and infants at 2.35 tesla. *Neuroradiology* 1991; **33**: 223–9.
85. DeVeber G, Andrew M, Adams C, *et al.* Cerebral sinovenous thrombosis in children. *N Engl J Med* 2001; **345**: 417–23.
86. Carvalho K, Bodensteiner J, Connolly P, *et al.* Cerebral venous thrombosis in children. *J Child Neurol* 2001; **16**: 574–85.
87. Lynch J, Hirtz D, deVeber G, *et al.* Report of the National Institute of Neurologic Disorders and Stroke Workshop on Perinatal and Childhood Stroke. *Pediatrics* 2002; **109**: 116–23.
88. DeVeber G. Arterial ischemic strokes in infants and children: an overview of current approaches. *Semin Thrombosis Hemostasis* 2003; **29**: 567–73.
89. Sebire G, Tabarki B, Saunders DE, *et al.* Cerebral venous thrombosis in children: risk factors, presentation, diagnosis, and outcome. *Brain* 2005; **128**: 477–89.
90. Kirton A, deVeber G. Cerebral palsy secondary to perinatal ischemic stroke. *Clin Perinatol* 2006; **33**: 367–86.
91. Fitzgerald K, Williams LS, Garg BP, *et al.* Cerebral sinovenous thrombosis in the neonate. *Arch Neurol* 2006; **63**: 405–9.
92. Barnes C, deVeber G. Prothrombotic abnormalities in childhood ischaemic stroke. *Thromb Res* 2006; **118**: 67–74.
93. Ehtisham A, Stern B. Cerebral venous thrombosis: a review. *Neurologist* 2006; **12**: 32–8.
94. Huang A, Robertson R. Spontaneous superficial parenchymal and leptomeningeal hemorrhage in term neonates. *AJNR Am J Neuroradiol* 2004; **25**: 469–75.
95. Govaert P, Vanhaesebrouck P, de Praeter C. Traumatic neonatal intracranial bleeding and stroke. *Arch Dis Child* 1992; **67**: 840–5.
96. Castillo M, Fordham LA. MR of neurologically symptomatic newborns after vacuum extraction delivery. *AJNR Am J Neuroradiol* 1995; **16**: 816–18.
97. Odita JC, Hebi S. CT and MRI characteristics of intracranial hemorrhage complicating breech and vacuum delivery. *Pediatr Radiol* 1996; **26**: 782–5.
98. Kleinman PK, Barnes PD. Head trauma. In Kleinman PK, ed., *Imaging of Child Abuse*, 2nd edn. St Louis, MO: Mosby-Year Book, 1998.
99. Alexander J, Leveno K, Hauth J, *et al.* Fetal injury associated with cesarean delivery. *Obstet Gynecol* 2006; **108**: 885–90.
100. Doumouchtsis S, Arulkumaran S. Head trauma after instrumental births. *Clin Perinatol* 2008; **35**: 69–83.
101. Teixeira J, Zimmerman R, Haselgrove J, *et al.* Diffusion imaging in pediatric central nervous system infections. *Neuroradiology* 2001; **43**: 1031–9.
102. Jan W, Zimmerman R, Bilaniuk L, *et al.* Diffusion-weighted imaging in acute bacterial meningitis in infancy. *Neuroradiology* 2003; **45**: 634–9.
103. DeVries L, Verboon-Maciolek M, Cowan F, *et al.* The role of cranial US and MRI in the diagnosis of infections of the central nervous system. *Early Hum Dev* 2006; **82**: 819–25.
104. Hoon AH. Neuroimaging in cerebral palsy: patterns of brain dysgenesis and injury. *J Child Neurol* 2005; **12**: 936–9.
105. Rodriguez D, Young Poussaint T. Neuroimaging of the child with developmental delay. *Top Magn Reson Imaging* 2007; **18**: 75–92.
106. Valk J, van der Knapp MS. Toxic encephalopathy. *AJNR Am J Neuroradiol* 1992; **13**: 747–60.
107. van der Knaap MS, Valk J. *Magnetic Resonance of Myelination & Myelin Disorders*, 3rd edn. New York, NY: Springer, 2005.
108. Barker P, Horska A. Neuroimaging in leukodystrophies. *J Child Neurol* 2004; **19**: 559–70.
109. Vanderver A. Tools for diagnosis of leukodystrophies and other disorders presenting with white matter disease. *Curr Neurol Neurosci Rep* 2005; **5**: 110–18.
110. Murakami Y, Yamashita Y, Matsuishi T, *et al.* Cranial MRI of neurologically impaired children suffering from neonatal hypoglycemia. *Pediatr Radiol* 1999; **29**: 23–7.
111. Alkalay A, Flores-Sarnat L, Sarnat H, *et al.* Brain imaging findings in neonatal hypoglycemia. *Clin Pediatr* 2005; **44**: 783–90.
112. Barkovich A, Ali F, Rowley H, *et al.* Imaging patterns of neonatal hypoglycemia. *AJNR Am J Neuroradiol* 1998; **19**: 523–8.
113. Govaert P, Lequin M, Swarte R, *et al.* Changes in globus pallidus with (pre) term kernicterus. *Pediatrics* 2003; **112**: 1256–63.
114. Dublin A, Hald J, Wootton-Gorges S. Isolated sulfite oxidase deficiency: MR imaging features. *AJNR Am J Neuroradiol* 2002; **23**: 484–5.